Journal of Geophysical Research: Oceans

RESEARCH ARTICLE
10.1029/2018JC014270

Anticyclonic Eddies Connecting the Western Boundaries of Indian and Atlantic Oceans

R. Laxenaire[1], S. Speich[1], B. Blanke[2], A. Chaigneau[3,4,5], C. Pegliasco[3], and A. Stegner[1]

[1]Laboratoire de Météorologie Dynamique, LMD-IPSL, UMR 8539, École Polytechnique, ENS, CNRS, Paris, France, [2]Laboratoire d'Océanographie Physique et Spatiale, UMR 6523, CNRS, Ifremer, IRD, UBO, Brest, France, [3]Laboratoire d'Etudes en Géophysique et Océanographie Spatiales, UMR, CNES, CNRS, IRD, UPS, Toulouse, France, [4]Institut de Recherches Halieutiques et Océanologiques du Bénin, Cotonou, Benin, [5]International Chair in Mathematical Physics and Applications (UNESCO Chair), University of Abomey-Calavi, Cotonou, Benin

Key Points:
- New eddy tracking method including eddy merging and splitting improves assessments from satellite-mapped fields
- Agulhas Rings show very complex behavior with much longer lifespan and geographical reach than previously thought
- They play a major role in efficiently connecting western boundary currents of the South Indian and Atlantic Oceans

Supporting Information:
- Supporting Information S1
- Supporting Information S2
- Figure S1
- Figure S2
- Figure S3
- Figure S4
- Figure S5
- Figure S6
- Figure S7
- Figure S8
- Figure S9

Correspondence to:
R. Laxenaire,
rlaxe@lmd.ens.fr

Citation:
Laxenaire, R., Speich, S., Blanke, B., Chaigneau, A., Pegliasco, C., & Stegner, A. (2018). Anticyclonic eddies connecting the western boundaries of Indian and Atlantic Oceans. *Journal of Geophysical Research: Oceans*, *123*, 7651–7677. https://doi.org/10.1029/2018JC014270

Received 13 JUN 2018
Accepted 21 SEP 2018
Accepted article online 10 OCT 2018
Published online 5 NOV 2018

Abstract The Indo-Atlantic interocean exchanges achieved by Agulhas Rings are tightly linked to global ocean circulation and climate. Yet they are still poorly understood because they are difficult to identify and follow. We propose here an original assessment on Agulhas Rings, achieved by TOEddies, a new eddy identification and tracking algorithm that we applied over 24 years of satellite altimetry. Its main novelty lies in the detection of eddy splitting and merging events. These are particularly abundant and significantly impact the concept of a trajectory associated with a single eddy, which becomes less obvious than previously admitted. To overcome this complication, we have defined a network of segments that group together in relatively complex trajectories. Such a network provides an original assessment of the routes and the history of Agulhas Rings. It links 730,481 eddies into 6,363 segments that cluster into Agulhas Ring trajectories of different orders. Such an order depends on the affiliation of the eddies and segments, in a similar way as a tree of life. Among them, we have identified 122 *order 0* trajectories that can be considered as the major trajectories associated to a single eddy, albeit it has undergone itself splitting and merging events. Despite the disappearance of many eddies in the altimeter signal in the Cape Basin, a significant fraction can be followed from the Indian Ocean to the South Brazil Current with, on average, 3.5 years to cross the entire South Atlantic.

Plain Language Summary Mesoscale eddies are ubiquitous structures in the ocean and are one of the major sources of ocean variability. They play a crucial role in physically shaping the ocean general circulation, in transporting and mixing energy, chemicals, and other materials within and among ocean basins. This should be true, in particular, south of Africa where the largest mesoscale eddies, the so-called Agulhas Rings, are shed from the Agulhas Current into the Cape Basin conveying Indian warm and salty waters into the Southeast Atlantic Ocean. However, due to their small-scale and highly variable nature, ocean eddies are inadequately sampled and poorly reproduced in numerical models. Hence, we still lack a good assessment of their population and an appropriate understanding of their dynamics and exact role in the Earth's climate. We propose here an original assessment on Agulhas Rings achieved by a tracking algorithm that we applied over 24 years of satellite altimetry. Its main novelty lies in the detection of eddy separation and coalescence events that replace the concept of trajectories by the consideration of an eddy network. Such a network provides an original assessment of the routes and history of Agulhas Rings longer and more complex than previously described.

1. Introduction

Mesoscale eddies and meanders are ubiquitous structures in the ocean and are one of the major sources of ocean variability (Stammer, 1997; Wunsch, 1999). They are thought to contribute significantly to the transfer of heat, salt, mass, and biogeochemical properties across the World Ocean (McWilliams, 1985). South of Africa, large mesoscale eddies (Lutjeharms, 2006), the so-called Agulhas Rings, are shed from the Agulhas Current into the Cape Basin at the Agulhas Retroflection (Duncombe Rae, 1991; Gordon & Haxby, 1990; Lutjeharms & Ballegooyen, 1988; Lutjeharms & Gordon, 1987; Olson & Evans, 1986) transporting Indian waters into the Southeast Atlantic (Arhan et al., 1999, 2011; Ballegooyen et al., 1994; Garzoli et al., 1999) affecting the heat,

salt, and biogeochemistry of the Atlantic Ocean (Gordon et al., 1992; Lehahn et al., 2011; Paul et al., 2015; Villar et al., 2015). They participate in the Agulhas Leakage (Lutjeharms, 2006; Ruijter et al., 1999); the Indo-Atlantic interocean exchange of water that has a strong impact on the Atlantic Meridional Overturning Circulation (AMOC), influencing its strength (van Sebille & van Leeuwen, 2007; Weijer et al., 1999, 2002), stability (Weijer et al., 2001), and variability (Biastoch & Böning, 2013; Biastoch, Böning, & Lutjeharms, 2008). Therefore, the origins, number, and fate of Agulhas Rings are key elements in assessing global ocean circulation and its variations in a changing climate.

Since 1992, several altimetry satellites have revealed the richness, complexity, and some surface properties of mesoscale ocean dynamics (Chelton et al., 2011, 2007; Hernandez et al., 1995). Based on these data, a number of studies have estimated eddies and their trajectories, mainly from middle to high latitudes, using various automatic eddy detection algorithms (e.g., Ashkezari et al., 2016; Biastoch, Böning, & Lutjeharms, 2008; Chelton et al., 2011, 2007; Doglioli et al., 2007; Faghmous et al., 2015; Isern-Fontanet et al., 2006; Le Vu et al., 2018; Matsuoka et al., 2016; Mason et al., 2014; Nencioli et al., 2010; Qiu-Yang et al., 2016). All these detection methods are based either on physical criteria (such as the estimation of the Okubo-Weiss parameter; Okubo, 1970; Weiss, 1991) or geometrical properties of the flow. Several of these methods and eddy atlases are proposed to the scientific community and are made public. However, to our knowledge, none of them were quantitatively qualified against independent data. Efforts have been made to evaluate one or more methods, but this evaluation has been undertaken at a very local scale or using subjective assessments. Souza, De Boyer Montegut, and Le Traon (2011), for example, have attempted to compare and validate three different detection methods using current knowledge of South Atlantic eddies as independent criteria. Chaigneau et al. (2008) and Faghmous et al. (2015) compared their detection to structures identified by various experts. However, this procedure proved to be very sensitive, as experts often disagreed. Finally, Mkhinini et al. (2014) and Casanova-Masjoan et al. (2017) undertook a more objective, albeit still qualitative, assessment of the skill of their method by using respectively, 10 and 2 surface drifters trapped in specific anticyclonic eddies.

Using different eddy detection methods, several authors have attempted to reconstruct and analyze Agulhas Rings trajectories in and across the South Atlantic (e.g., Byrne et al., 1995; Gordon & Haxby, 1990; Souza, de Boyer Montégut, Cabanes, & Klein, 2011; Wang et al., 2015). In the published studies, most reconstructions of the trajectories of Agulhas Rings leaving the Cape Basin are identified initially well within the Cape Basin and not at the Agulhas Current Retroflection where they are believed to originate (e.g., Byrne et al., 1995; Guerra et al., 2018; Souza, de Boyer Montégut, Cabanes, & Klein, 2011; Wang et al., 2016, 2015). Taking into account the separation of an eddy into smaller structures, to which, in what follows, we will refer to as an eddy splitting event, Dencausse et al. (2010a) tracked the Agulhas Rings formed in the Agulhas Retroflection area and entering the Cape Basin. They have shown that such events are very frequent. Indeed, the ratio obtained between the number of trajectories formed after a split and the number of trajectories tracked from the Agulhas Retroflection is close to 1. This process has an impact on the concept of Agulhas Ring trajectories and on the number of Agulhas Rings formed per year (traditionally estimated between 3 and 6; e.g., Ballegooyen et al., 1994; Byrne et al., 1995; Goni et al., 1997; Gordon & Haxby, 1990). In fact, Dencausse et al. (2010a) have shown that up to 14 Agulhas Rings per year enter the Cape Basin. However, these authors have only followed Agulhas Rings in a very limited region without addressing the question of the impact of these eddy-eddy interactions on the recovery of the full extent of Agulhas Rings trajectories. For example, Schouten et al. (2002) showed that certain eddies formed in the Mozambique Channel or at the southern limit of Madagascar can, in addition to triggering Natal Pulses, be advected until the Retroflection region leading to shedding of an Agulhas Ring. Downstream from the Cape Basin, most of the Agulhas Rings described in the literature do not cross the South Atlantic entirely. To our knowledge, the only exceptions are a trajectory followed by Byrne et al. (1995) that reached 40°W near the American Margin and another by Guerra et al. (2018) that clearly drifted south along the Brazilian coast. All these individual regional pictures of Agulhas Ring trajectories must, in one way or another, be incorporated into a global vision taking into account the eddy-eddy interactions.

In this article, we present a new eddy detection and tracking algorithm applied to the 24-year satellite altimetry time series in a space domain covering the South Atlantic and Southwest Indian Oceans. The eddy detection and tracking steps of this new algorithm are a development of the geometric method of Chaigneau et al. (2008), Chaigneau et al. (2009), and Pegliasco et al. (2015). To obtain an objective measure of the capabilities of our method and the robustness of our eddy database, we have developed a systematic procedure that tests the presence and properties of eddies against a totally independent data set, so-called the *loopers*, which are upper-ocean eddies identified from surface drifters and provided by Lumpkin (2016).

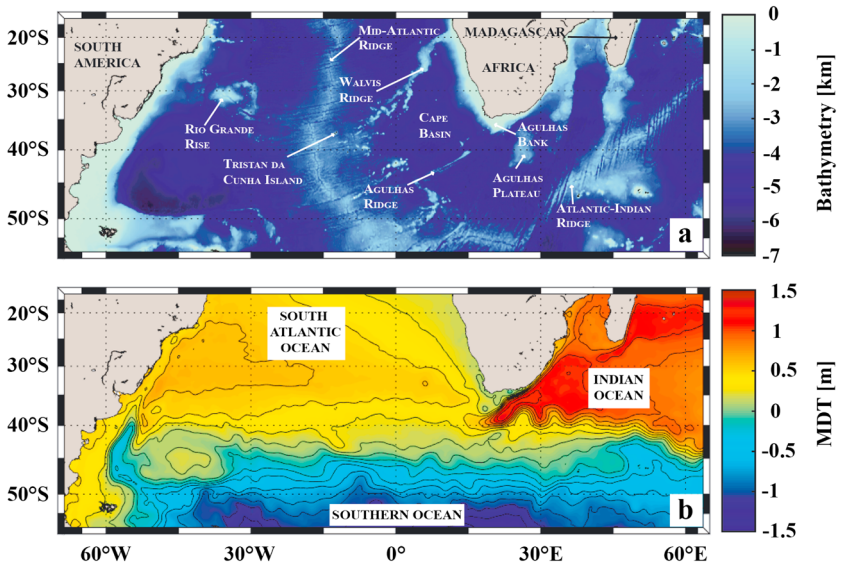

Figure 1. Study domain and (a) bathymetry from the ETOPO2 data set (Smith & Sandwell, 1997) and (b) mean dynamic topography (MDT; ; Duacs/AVISO+, 2014) with the main currents indicated.

While the method is developed and tested on all eddies detected in the domain of study, particular emphasis will be placed on the results concerning the Agulhas Rings. Indeed, the new eddy detection and tracking method gives access to an unprecedented assessment of the origin and fate of the Agulhas Rings and the Indo-Atlantic exchange of waters they carry out. Moreover, we will discuss their characteristics and variations along the trajectories in terms of various kinematic and dynamical properties that can be deduced from altimetry.

The paper is organized as follows. In section 2, the data we have used are described and the methods we have developed are presented. Validation and comparisons of our eddy detection algorithm with a published databases are presented in section 3. Section 4 focuses on the Agulhas Rings. We discuss their origins, their disappearance from the altimetry field, their trajectories, and statistics on the different properties of Agulhas Rings. In the last section, the results are discussed and we draw the main conclusions of this study.

2. Data and Methods

2.1. Satellite Altimetry Data

This study is based on more than 24 years (January 1993 to May 2017) of daily maps of delayed time absolute dynamic topography (ADT) and derived geostrophic velocity fields in the South Atlantic and Southeast Indian oceans [70°W to 65°E; 55°S to15°S] (see Figure 1). These maps are produced by Ssalto/Duacs and distributed by the Copernicus Marine Environment Monitoring Service (http://marine.copernicus.eu/) in the version released in April 2014 (DT14; ; Duacs/AVISO+, 2014; Pujol et al., 2016). They correspond to the gridded sea surface height (SSH) above the geoid calculated by combining all the data recorded by the satellites available among the 12 altimetric missions (Topex/Poseidon, ERS-1 and ERS-2, Jason-1, OSTM/Jason-2, SARAL/Altika, Cryosat-2, Envisat, Geosat, Haiyang-2A, Jason-3, and Sentinel-3A). Objectively mapped ADT is the sum of sea level anomalies (SLAs) and mean dynamic topography (MDT) maps, both referenced over a 20-year period in the Ssalto/Duacs 2014 version (Duacs/AVISO+, 2015). The improved data processing used in DT14 provides a better description of mesoscale activity than previously distributed products (Capet et al., 2014; Pujol et al., 2016).

Most published studies, which also include previous developments of the current method (Chaigneau et al., 2011; Pegliasco et al., 2015), have applied an eddy detection algorithm to SLA. This was essentially to avoid errors due to the imprecision of the definition of the Earth geoid. Recently, the availability of the latest version of MDT (MDT CNES-CLS13; ; Rio et al., 2014), calculated from a 20-year average (1993–2012) of altimetry data and a geoid obtained by correcting the Gravity and Ocean Circulation Experiment model with dynamic height and velocity estimates derived from in situ observations (Rio et al., 2011, 2014) provides a better estimate of the geopotential surface height of the ocean, which significantly improves ADT and associated

ocean dynamics (Rio et al., 2014). Like Halo et al. (2014), we choose to use ADT instead of SLA maps because the latter are strongly affected by the position and displacement of large SSH gradients associated with intense currents and quasi-stationary meanders and eddies, all included in MDT as shown in Figure 1b. This is particularly true for the Agulhas Current system. In fact, small shifts relative to average current positions can generate artificial dipoles of positive and negative SLAs. These dipoles are identified as two eddies in SLA, whereas they are not detected in ADT. In addition, ADT is directly associated with important physical variables such as ocean currents and the geostrophic stream function.

2.2. The Ocean Eddy Detection and Tracking Algorithms (TOEddies)

This eddy detection algorithm is an evolution of the method proposed and developed by Chaigneau et al. (2009, 2008). It is based on the key assumption that for geostrophic eddies, the streamlines correspond to the closed contours of SSH. The eddy detection algorithm is a two-step process: it identifies the occurrence of eddies before deriving their trajectories.

First and foremost, the method identifies the local extrema (maxima and minima) of ADT as possible eddy centers. Then, it looks for the outermost closed ADT contours around each extremum containing at least 4 grids points. The module of the ADT difference between the extremum and this contour defines the detected eddy amplitude, which is considered as a proxy of the eddy (surface) signature. Cipollone et al. (2017) showed that two close extrema can be dependent and thus defined a minimum distance between extrema so that they are considered as possible eddy centers. In this study, we introduced as a parameter of the eddy detection method, a minimum threshold for the amplitude of the eddy extrema. This ensures that a detected extremum can be considered as an eddy center. Extrema associated with an amplitude below the threshold will not be a constraint for the detection of the outermost closed ADT contours associated with others extrema.

This parameter (the eddy amplitude threshold) can be interpreted as an eddy *persistence*, a notion of topological simplification introduced by Edelsbrunner et al. (2002) and Edelsbrunner and Harer (2010), which has been widely used since (e.g., Tierny et al., 2018). The persistence criterion by reducing the number of extrema aims to avoid the overrepresentation of dynamically insignificant structures because it should prevent the artificial separation of a large eddy into two or more smaller elements. Therefore, in the following, the amplitude threshold parameter will be called persistence to distinguish it from the minimum amplitude criterion that has been widely used in the literature (e.g., Chelton et al., 2011). Faghmous et al. (2015) showed that the minimum amplitude criterion, with its typical value of 1 cm, could lead to the loss of significant structures. A sensitivity test on eddy persistence is presented in Table A1 according to the method presented in section 3. It shows that a nonzero value for the persistence parameter (set to 1 mm) increases the number of structures as well as the ability of our detection method to define eddies. However, a further increase in the persistence parameter value does not show significant improvements in the eddy detection capability. This is why we have set this parameter value to 1 mm. Note that this value, which acts somewhat like a low-pass filter, is considerably smaller than the resolution of 1 to 2 cm defined in the literature as the nominal resolution of satellite altimetry.

The detected ADT extrema that pass the persistence threshold are each identified as the center of an eddy if there is at least one closed ADT contour containing only one local extreme and including at least four connected grid points. The size of each eddy is then characterized by two distinct radii. The equivalent outermost radius, R_{out}, which corresponds to the radius of a disk having the same area (A_{out}) as that delimited by the outermost closed contour. Its value is given by the equation

$$R_{out} = \sqrt{\frac{A_{out}}{\pi}} \tag{1}$$

However, the outermost closed contour is often strongly distorted by the surrounding flow and interactions with others mesoscale structures. For this reason, we also used, as a reference variable for the method, the contour corresponding to the ADT contour along which the mean azimuthal geostrophic velocity is maximum (V_{max}). This limit, called the *characteristic contour* in this study, tends to be more robust and coherent in time than the outermost contour. We then defined the maximum speed radius, R_{Vmax}, associated with the area delimited by the characteristic contour. R_{Vmax} is always smaller or equal to R_{out}. It characterizes the eddy core and allows easy comparisons with in situ measurements such as ADCP transects or drifter trajectories (Ioannou et al., 2017; Mkhinini et al., 2014). The accuracy of each eddy center (associated with a local ADT extremum) is limited by the ADT field defined at a horizontal resolution of 1/4°. Because of this precision limit, we chose to

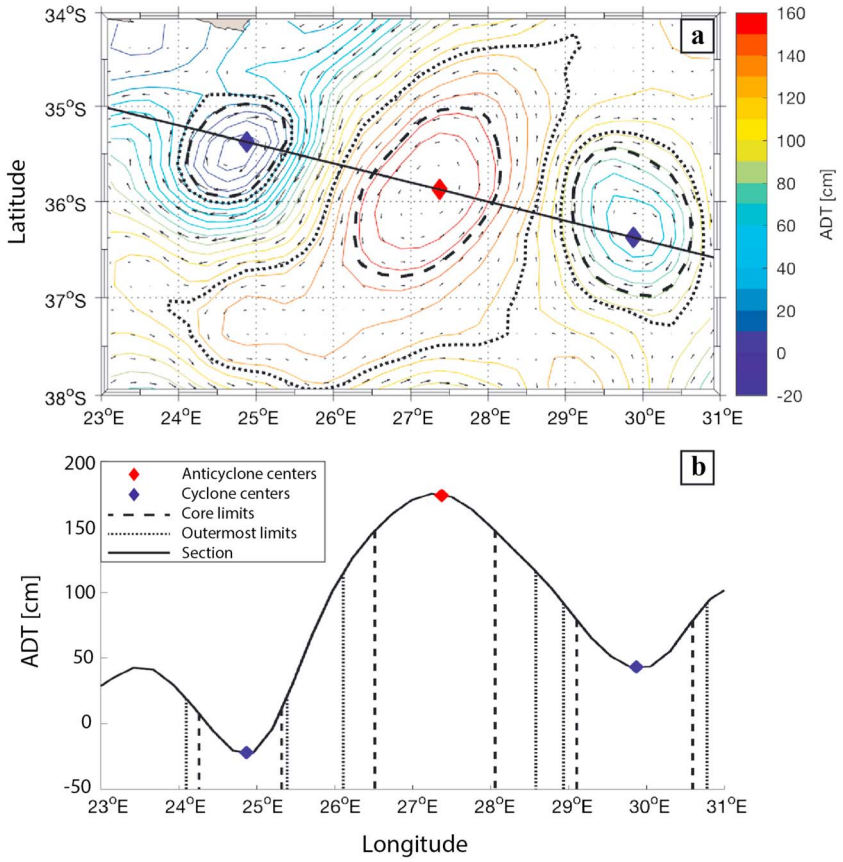

Figure 2. Example of eddies detected near the Agulhas Current on 23 March 2000. Two cyclones and one anticyclone are shown in (a) an absolute dynamic topography (ADT) map and (b) in terms of ADT amplitude along a section crossing the extrema of the eddies detected in (a). For each eddy, the ADT contours where the azimuthal speed is maximum (eddy core limit definition: dashed lines) and the outermost closed contour (eddy outer limit definition: dotted line) are shown. ADT isolines with 10-cm intervals and the geostrophic velocity vectors distributed by AVISO are superimposed in (a).

use the centroid of the area associated with the eddy core as the center of each structure. Indeed, this variable is less affected by the ADT resolution. An example of the two boundaries of two cyclones and an anticyclone and their eddy centers associated to the ADT grid is shown in Figure 2.

The vortex surface Rossby Number (Ro) is used to compare eddy characteristics in different regions (e.g., Chelton et al., 2011; Le Vu et al., 2018; Mkhinini et al., 2014), as it is a proxy of the surface intensity of the dynamic core (equation (2), where f is the Coriolis parameter).

$$Ro = \frac{V_{\max}}{fR_{\mathrm{Vmax}}} \tag{2}$$

In a second step of the eddy detection method, a complete and continuous set of eddy trajectories is recovered by following the paths of the eddies between successive ADT maps. Taking advantage of daily AVISO fields, the method relies on the fact that mesoscale eddies move slowly (displacements of less than 10 km/day; see also ; Chelton et al., 2011) relative to their radii that typically extend from 20 to 200 km (Carton, 2001). This ensures that the areas covered by the same eddy for two consecutive days overlap. This overlap can be used to track eddies (Pegliasco et al., 2015). We use the characteristic contour (R_{Vmax}), less distorted than the outermost contour, to define the surface of the eddy core. However, in sporadic cases, the eddy surfaces defined by R_{Vmax} for two consecutive days do not overlap. Hence, we set the method to check in parallel the overlap of the eddy surface defined by the outermost contour. To avoid false eddy associations, a minimum percentage of overlap is required when considering this larger eddy surface. This overlap threshold, which is calculated as the ratio of the overlap area to the area of the smaller of the two eddies, provides robust eddy tracking (Figure 3a). Indeed, assuming a small circular eddy with a radius of 20 km moving at a speed of 10 km/day,

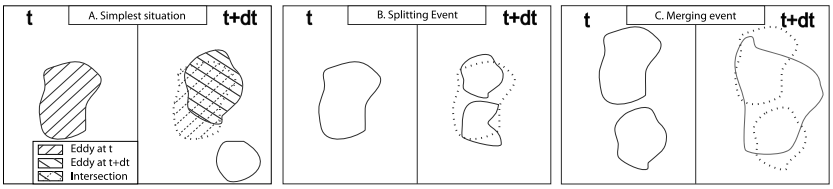

Figure 3. Schematic diagram of the eddy tracking step of the algorithm. (a) Simplest situation where a single eddy is identified at the two different time intervals, t and $t + dt$. The area of the two eddy occurrences and their overlapping surface are shown, the latter in the form of a hatched surface. (b) Splitting event. (c) Merging event. Although the overlap threshold is applied in (b) and (c), these areas have not been represented to ensure readability of the figures.

73% of its surface will overlap for two days. Therefore, the threshold should be less than 70%. Unfortunately, due to the small number of long life trajectories identified from drifting buoys (see section 3), this parameter could not be tested quantitatively. Instead, qualitative trajectory inspections using different percentages of the overlap threshold (0%, 25%, and 50%) were undertaken. Due to the need for confidence in the method and the fact that comparisons between drifting buoys and eddy trajectories derived from altimetry showed suspicious trajectories using small overlap threshold values, the value of 50% was chosen. As some authors have already documented (e.g., Chaigneau et al., 2008; Chelton et al., 2011; Faghmous et al., 2015; Le Vu et al., 2018), eddies can disappear from altimetry maps for several days as a consequence of the heterogeneous distribution of the altimetry tracks. To take into account this possible lack of detection, an eddy, which has no parents in the previous time step or children in the following time step, is allowed to continue to exist if its disappearance does not last more than five consecutive days.

Nonlinear interactions between distinct eddies or between eddies and topography are some of the processes that can induce the splitting or merging of eddies. These processes have been theoretically supported (e.g., Drijfhout, 2003; Melander et al., 1988; Simmons & Nof, 2000) and observed (e.g., Cresswell, 1982; Isoda, 1994; Sangrà et al., 2005; Schultz Tokos et al., 1994). The TOEddies algorithm belongs to the very few eddy detection and tracking algorithms (Le Vu et al., 2018; Matsuoka et al., 2016; Qiu-Yang et al., 2016; Yi et al., 2014) that consider both processes. It combines the separation of a large eddy with two or more smaller eddies in the case of splitting (see Figure 3b) and relates the coalescence of two or more small eddies into a larger eddy in the case of merging (see Figure 3c).

To take these processes into account, a relationship tree is created associating each eddy with its potential parents and children. Independent eddy trajectory segments are constructed by scanning this tree. These segments are trajectories that link the eddy positions between the merging and splitting events. Therefore, each segment begins either after the detection of a new eddy or after the merging of two eddies or the splitting of an eddy into two or more smaller eddies and ends the time step before a new eddy-eddy interaction or when the eddy disappears from the altimetry maps.

The next step is to combine these segments to reconstruct the main eddy trajectories. To do this, the method first evaluates the overlap of the eddy surfaces associated with the characteristic contours (A_{Vmax}). In many cases, only two segments can be associated. A main eddy trajectory is defined from their assembling. In the next step, the method searches for overlapping eddy surfaces associated with R_{out}. This step is used to define trajectories that split from or merge with the eddy main trajectory. During eddy merging and splitting events, an eddy defined by the surfaces associated with R_{Vmax} can be associated with more than one segment. In these cases, we use a cost function to identify the main eddy trajectories. Using a cost function to define eddy trajectories is a relatively standard approach (e.g., Chaigneau et al., 2009, 2008; Frenger et al., 2015; Le Vu et al., 2018; Penven et al., 2005). The cost function we defined (equation (3)) takes into account the distance between the successive eddies and the change in eddy core surface properties (i.e., within the R_{Vmax} limit). Independent segments that minimize the cost function are linked together. The resulting long series of segments is identified as the main eddy trajectory. The remaining trajectories are classified as the result of an eddy splitting from the main trajectory or an eddy merging with the main trajectory.

$$CF = \sqrt{\left(\frac{\Delta\text{Center} - \overline{\Delta\text{Center}}}{\sigma_{\Delta\text{Center}}}\right)^2 + \left(\frac{\Delta Ro - \overline{\Delta Ro}}{\sigma_{\Delta Ro}}\right)^2 + \left(\frac{\Delta R_{\text{Vmax}} - \overline{\Delta R_{\text{Vmax}}}}{\sigma_{\Delta R_{\text{Vmax}}}}\right)^2} \quad (3)$$

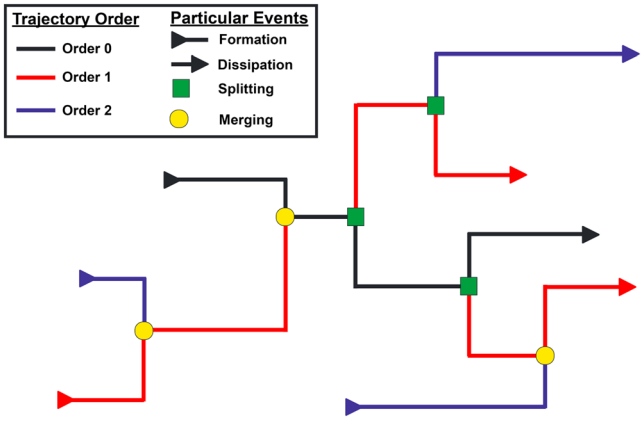

Figure 4. Schematic of a simple network of trajectories up to order 2. This network is characterized by four formations, four disappearances, and three merging and splitting events. With each merging and splitting, the cost function is applied to follow the main trajectory by associating a segment with a higher order.

The cost function we used (called CF in the following) is presented in equation (3) where, for a difference $\Delta\alpha$ of the generic variable α between two independent segments, $\overline{\Delta\alpha}$ and $\sigma_{\Delta\alpha}$ denote, respectively, the mean and the standard deviation of the differences. They are calculated between all pairs of a parent eddy associated with a single child eddy and conversely. The variables we used in defining the cost function are based on the work of Le Vu et al. (2018). In addition, we prescribed the mean and the standard deviation estimates of the variables used in the cost function following Pegliasco et al. (2015) to ensure similar ranges of variation for every variable to assign them the same weight.

In order to reduce the effect of spurious variations in the gridded ADT product, the values used in CF are averaged over the last or the first 7 days of each independent segment in the case of eddy merging and splitting, respectively. In this way, the CF can, for example, identify two trajectories that merge for only few time steps before splitting again. In this case, this event is identified as an interaction instead of a real merging followed by a splitting. This is close to the neutral interactions presented in Le Vu et al. (2018) with an interaction period set at 5 days. To limit the number of short life segments that connect the trajectories or increase the number of eddy-eddy interactions, each independent segment must last more than 4 weeks to be taken into account. This ensures that the segments of a trajectory are consistent over a relatively long period of time.

Taking into account eddy merging and splitting, the meaning of an eddy trajectory radically changes the traditional view of mesoscale eddies moving as isolated and coherent structures from their formation zone to their dissipation zone. This is why we propose here to characterize the evolution of these structures not in terms of eddies, but by a network of trajectories. Such a network is composed of several branches identified as independent segments that begin either with a merging or splitting event or with the formation of a new structure, and end with another merging or splitting event or with the disappearance of the structure in the altimetry maps.

To match the in situ observation of isolated eddies with the associated trajectory network, we propose assigning an order to each segment of a main trajectory as shown in Figure 4. In this formalism, the *order 0* of the trajectory network is the main trajectory identified by applying the CF for each occurrence of merging and splitting. With *order 1*, we assign segments that are linked to the main trajectory either by an eddy splitting or an eddy merging. Similarly, the *order 2* refers to segments that are associated with eddy merging or splitting with order 1 trajectories, etc. This recursive classification in ordered trajectories continues until no new orders are detected. Each network is therefore associated with an order n of trajectories. The order 0 of each network of trajectories is defined according to the target of the study as, for example, the assessment of the origin and fate of a mesoscale eddy identified by in situ observations or a global view of mesoscale eddies formed in a particular region of the ocean, such as the Agulhas Rings.

2.3. The AVISO+ Mesoscale Eddy Trajectory Atlas

Chelton et al. (2011) is the most publicly available atlas cited for mesoscale eddies automatically defined from satellite altimetry data. A new version of this algorithm has been implemented by Schlax and Chelton (2016), which is used by SSALTO/DUACS to produce the Mesoscale Eddy Trajectory Atlas (hereafterMETA2017; Duacs/AVISO+, 2017) distributed by AVISO+ (http://www.aviso.altimetry.fr/) with support from CNES, in collaboration with Oregon State University with support from NASA.

The META2017 detection method is based on the geographical properties of the *two-sat-merged* SLA maps after application of a spatial high-pass filter. The META2017 algorithm identifies anticyclonic (cyclonic) eddies by locating the pixel at a local maximum (minimum) of SLA and successively finding all neighboring pixels with SLA values above (below) a sequence of decreasing (increasing) thresholds following the *growing method* of Williams et al. (2011). This *growth* of the eddy structure continues until one of the five criteria defining a compact and coherent structure is violated. The five criteria used are chosen to generate eddies statistically similar to those obtained by Chelton et al. (2011). Eddies with an amplitude of less than 1 cm are not

Table 1
Parameters of the Six Data Sets Tested Against the Independent LU16 Eddy Atlas Derived From Surface Drifter Buoys

Data set name	Persistence or minimum Amplitude (mm)	Minimum surface (%)	Lifetime (week)
SLA_raw	1	N/A	N/A
ADT_raw	1	N/A	N/A
TOEddies	1	50	4
TOEddies_rad	1	50	4
META2017	10	N/A	4

Note. Each row corresponds to a different data set for which the version and the type of satellite altimetry maps used for the detection is specified. The suffix *_raw* is added when the 4-week threshold on lifetime eddy segments is not applied. The suffix *_rad* refers to the results of the LU16-TOEddies collocation performed using the eddy radius instead of the eddy area criterion. N/A (not applicable) is added when a parameter is not relevant for a data set.

included in META2017. This algorithm is described in detail in Schlax and Chelton (2016) and the eddy atlas in Duacs/AVISO+ (2017).

One of the main differences between TOEddies and META2017 algorithms is the eddy tracking step. META2017 applies a cost function to the eddies in the successive maps in an elliptical search area whose size depends on latitude. TOEddies, instead, requires eddy areas to overlap. The META2017 cost function compares the amplitude and position of the identified eddies with those of the next time step. It then selects only one structure to define the trajectory of the eddy. It therefore does not take into account eddy merging nor eddy splitting processes. In META2017, only eddies of at least 4 weeks are documented.

2.4. Loopers Recovered From Surface Drifters

The robustness of the method and the related parameter choices were evaluated by comparing our results with independent in situ data. To do this, we used the eddies identified by (Lumpkin, 2016, hereafter LU16) from the Global Drifter Program quality-controlled surface drifters data (Lumpkin & Pazos, 2007) over the world ocean from February 1979 to July 2017 (http://www.aoml.noaa.gov/phod/loopers/index.php). In LU16, the eddies are automatically identified as *looping* trajectories of drifters buoys reconstructed from the four positions they send each day. To do this, the methodology initially introduced by Veneziani et al. (2004) and developed by Griffa et al. (2008) and LU16 is used. In this method, the spin Ω of each trajectory that can be related to the vorticity of the Eulerian fluid field for a particle following the rotation of a solid body (Veneziani et al., 2004) is computed at each position. Using the properties of circular motion, we can estimate both the period and radius of these loop trajectories. We refer to LU16 for a complete description of the method.

It should be noted here that LU16 underestimates the total number of eddies because it only accounts for eddies captured by the small number of drifting buoys deployed in the ocean. In addition, LU16 estimates only the radius of the loops of each drifter, which may be different (essentially smaller) than the actual radius of the eddy sampled. Indeed, it has been shown by Chaigneau and Pizarro (2005), by comparing the eddies detected from altimetry with drifting buoys, and by Pegliasco et al. (2015), with Lagrangian profiling floats that, on average, these instruments sample the eddy at two thirds of the R_{out}, which corresponds to a random sampling of a disk with a radius equal to R_{out}. Therefore, to avoid erroneous comparisons of eddy radii, only LU16 eddy center positions are used. We followed LU16 to evaluate such a center: it is defined as the mean center position of the buoy's looping trajectory during a rotation period. The instantaneous radius of each eddy detected by LU16 is computed as the distance between the estimated position of the eddy center and the position of the drifter along its loop.

3. Validation and Comparison of Eddies Data Sets

3.1. The Validation Approach

For validation purposes, a daily collocation was performed between the five eddy data sets listed in Table 1 in the South Atlantic-Southeast Indian geographical domain [70°W to 65°E; 55–15°S] during the period 1 January 1993 to 31 December 2016. Only LU16 eddies whose center is at least 5° away from the limits of the geographical domain are taken into account. Indeed, eddies close to the limits of the domain may not be

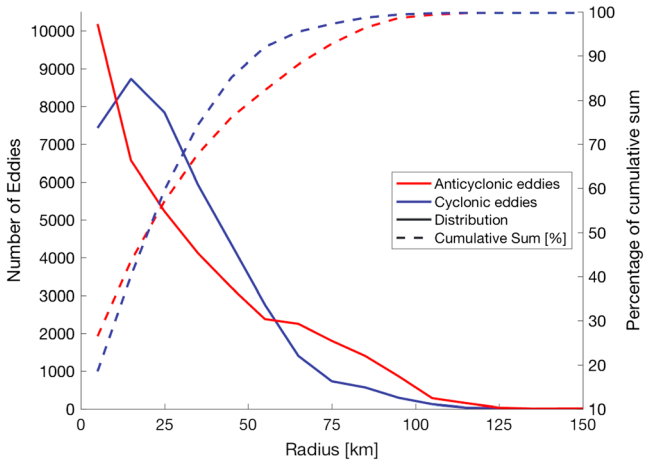

Figure 5. Number of eddies (on the ordinate) identified from surface drifting buoys by Lumpkin (2016) and used to validate the robustness of the eddies identified by the TOEddies algorithm shown as function of their radii (on the abscissa). The radii are sampled every 10 km. These numbers are computed separately for anticyclonic and cyclonic eddies.

detected by TOEddies. In what follows, LU16 will be the reference data set. Within this framework, only the trajectories of drogued surface drifters for which a position of an eddy center could be estimated and whose radius is less than 300 km are chosen, which constitutes a reasonable upper limit for mesoscale ocean eddies (Carton, 2001).

This selection results in 38,503 anticyclonic and 40,251 cyclonic eddy centers identified by LU16 in the study area. Only surface drifters trapped in a structure for more than a week are used here for the validation of eddy trajectories. Only 431 anticyclonic and 414 cyclonic LU16 trajectories last more than 7 weeks in the region. This number is relatively small because we only took into account LU16 loopers associated with radii less than 300 km. Therefore, the LU16 trajectories used in this study are shorter than originally estimated.

In Figure 5 the number of LU16 eddies available for cross detection are plotted according to their radii that we recalculated. The resulting LU16 mean radii are between 0 and 10 km for anticyclones and between 10 and 20 km for cyclones. The number of eddies in each size interval decreases as the size of the structure increases. The median is about 25 km for both types of eddies. Ninety percent of cyclones have a radius less than 56 km, and 90% of anticyclones have a radius less than 74 km. Fewer than 1% of cyclones and 2% of anticyclones have a radius greater than 100 km.

As mentioned earlier, the estimated radii of the LU16 loopers cannot be an estimate of the true size of mesoscale eddies, as surface drifters loop along circles that are smaller than the eddy cores. However, they can be used to define a minimal size for mesoscale eddies. Half of the LU16 distributions have radii greater than 25 km, which corresponds approximately to the pixel size of 1/4° horizontal resolution in altimetry gridded products. It is therefore reasonable to use LU16 loopers to validate the eddies detected in the altimetry fields. Since only a small fraction of the LU16 eddies have a radius greater than 100 km, we have set the maximum radius to be taken into account at this value.

For validation, we consider that two eddies are colocated (i.e., a valid cross detection) if the center of a LU16 eddy falls in the area occupied by an eddy of the same sign detected by one of the altimetry-based algorithms. An example of this matching is shown in Figure 6. For data sets that do not explicitly provide the eddy contour (e.g., META2017), a correspondence exists if the center of one LU16 eddy and the center of one eddy in the other data set is within a distance smaller than the eddy radius defined in such data set.

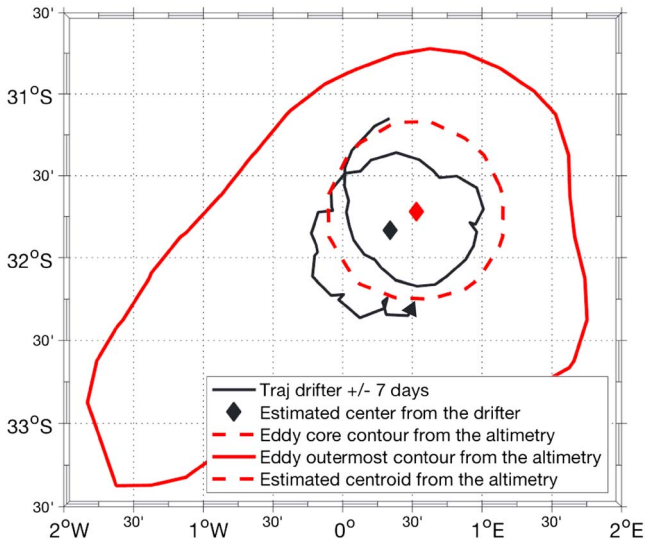

Figure 6. Example of cross detection of eddies for 12 December 2012 where an eddy identified from a surface drifter trajectory by LU16 (in black with a diamond symbol locating its center) and an anticyclone detected in the TOEddies Atlas (red contours for its outer limit and its maximum speed core with a red diamond symbol locating its center) overlap.

We implemented the collocation with LU16 loopers to the data sets listed in Table 1. The first four data sets correspond to the TOEddies detection algorithm applied to the two different altimetry maps (SLA and ADT) and parameter thresholds. The first three letters of these data sets indicate the type of map used as input. Moreover, while in TOEddies we apply a 4-week threshold on the life of eddy segments that filters out segments associated with short-lived eddies, the suffix *_raw* is added when this filtering is not applied. The suffix *_rad* refers to the results of LU16-TOEddies collocation performed in the same manner as LU16-META2017, that is, using the eddy radius instead of the eddy area criterion.

3.2. Validation of the Eddy Detection and Tracking Algorithms

In the following we summarize the main results of the cross validation between LU16 and the different eddy satellite altimetry databases listed in Table 1, as well as the different threshold parameters and a thorough comparison with the META2017 atlas. Details of validation and comparisons are discussed in Appendix A .

All data sets tested (Table 1) show both a decrease in error and an increase in detection efficiency for LU16 eddies with large radii (see Table 2). This

Table 2
Detection and Collocation Matching Statistics With LU16 Eddies

Data Set	Number Eddies anti/cyclo (10^6)	Sum area max anti/cyclo (10^{10} km^2)	Sum area out anti/cyclo (10^{10} km^2)	Match anti max/out (%)	Mismatch anti max/out (%)	Match cyclo max/out (%)	Mismatch cyclo max/out (%)
SLA_raw	4.3/4.5	4.3/4.2	7.7/7.6	62/69	2/4	72/78	1/2
ADT_raw	3.2/3.3	3.2/2.8	5.2/4.6	66/71	2/3	71/75	1/2
TOEddies	2.4/2.5	2.8/2.5	4.7/4.2	63/67	2/3	65/69	1/2
TOEddies_rad	2.4/2.5	2.8/2.5	4.7/4.2	60/63	1/3	64/65	1/4
META2017	1.8/1.8	4.1/4.1	N/A/N/A	50/N/A	3/N/A	53/N/A	3/N/A

Note. max refers to the eddy contours associated with their maximum speed, while *out* refers to their outer contours. The percentages indicate the proportions of eddies by polarity as defined in LU16. Anti and cyclo mean, respectively, anticyclones and cyclones. N/A (not applicable) is added when a parameter is not relevant for a data set.

is most likely due both to the limited spatial resolution of satellite altimetry and its limited ability to capture small structures (e.g., Chelton et al., 2011) and also to the lower probability that drifting buoys are captured in small eddies rather than in large eddies. However, it should also be noted that LU16 eddy radii may provide an underestimate of the actual size of structures. Indeed, drifting buoys are drawn by the movement of the upper ocean at different distances from the center of the eddy and they do not necessarily move along the outer eddy edge of the eddy or along its maximum velocity. Indeed, it has been shown that drifters sample randomly eddy structures (Chaigneau & Pizarro, 2005).

Test results show that the TOEddies algorithm detects significantly fewer structures when applied to ADT maps than SLA maps. Consequently, the total area occupied by the eddies identified on ADT maps is about 30% less than on SLA maps. Compared to LU16, the TOEddies identification of anticyclones on the ADT maps shows better skill, especially when eddies are identified by the maximum velocity contour. Conversely, cyclones are better identified from SLA maps. However, the fact that the number of eddies detected in ADT maps is significantly lower than that in SLA maps convinced us to use the former. We also noted that detection efficiency increases significantly when eddies are defined by their actual contours instead of assuming circular eddies with assigned equivalent radii.

The comparison of TOEddies with META2017 shows that the former has better skill in both stages, eddy detection and eddy tracking. TOEddies detects more eddies, and their size is smaller than those detected by META2017 (Figure 7). It also shows particularly good performance in identifying large structures (with a radius greater than 40 km). Figure 8 shows that for a 25-km radius (which represents the average radius of the LU16 loopers, Figure 5, and the average grid size of the altimetry maps) more than 65% of the eddies are identified by TOEddies, whereas they represent only 48% (52%) for the anticyclones (cyclones) in META2017. Finally, 50% of the TOEddies trajectories correspond to those of LU16. Therefore, the results of the validation and skill assessment of TOEddies against another eddy detection method or independent data give us confidence in our algorithm in the study area. To be noted that TOEddies eddies are close in size to the regional first baroclinic Rossby Radius of deformation (Figure 7).

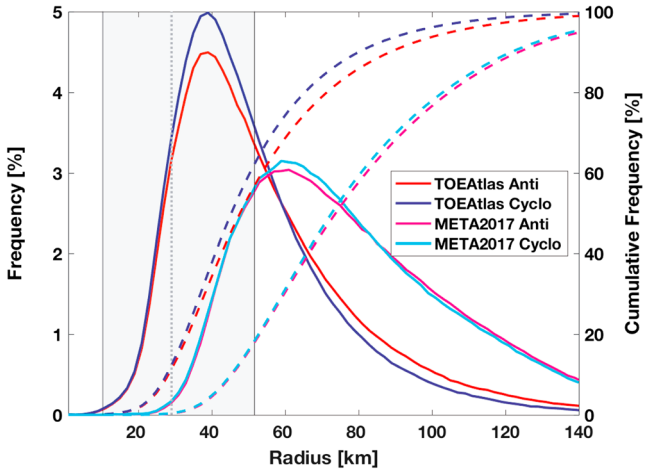

Figure 7. Histograms (solid lines) and cumulative frequency (dashed lines) of the eddy R_{max} for TOEddies (red and blue lines) and META2017 (pink and light blue lines) computed over 2-km intervals. The vertical dotted line is the mean first baroclinic Rossby radius (L_R) of deformation in the area and the gray dashed area limits the 10th and 90th percentiles. The baroclinic Rossby radius of deformation is computed by applying the Chelton et al. (1998) method on the World Ocean Database (Boyer et al., 2013) averaged over 7 years (i.e., 2005 to 2012).

4. Results of the TOEddies Method Applied to Agulhas Rings

4.1. Identification of Agulhas Rings and Distribution of the Associated Trajectories

TOEddies has identified, overall, more than 3 million eddies in the daily ADT maps in the selected Indo-Atlantic domain and for the given time period (>24 years). This corresponds to 120,000 anticyclonic trajectory segments identified from the full tree of segments, using the cost function.

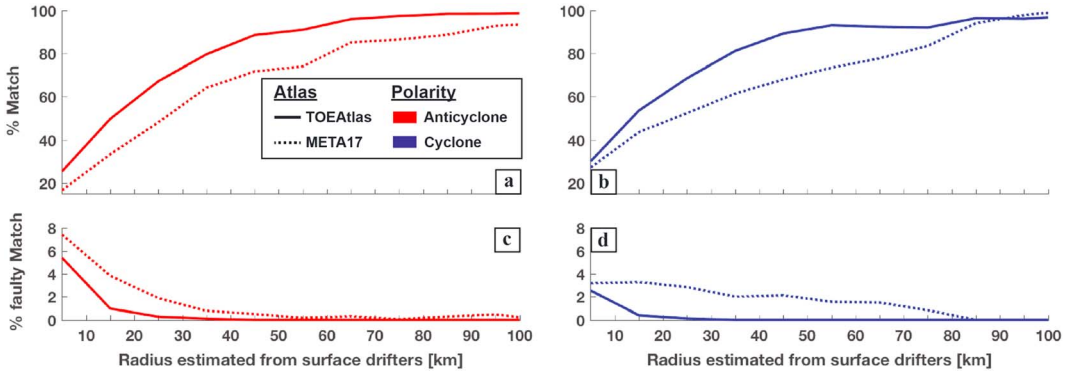

Figure 8. Percentage of matching (panels a and b) and missmatching (panels c and d) of LU16 anticyclonic and cyclonic eddies with TOEddies (solid lines) and META2017 (dashed lines) eddies as a function of LU16 eddy size. Values are expressed as a percentage of LU16 eddies collocated at 10-km intervals. We consider that eddies match if their polarity in LU16 and in the atlases based on altimetry is the same. When the polarities of the collocalized eddies differ, this is counted as a mismatch. Anticyclones are in red; cyclones are in blue.

These figures are reduced to 2.5 million eddies and 30,000 segments after application of the minimum 4-week lifetime threshold. Among these eddies and segments, the Agulhas Rings (hereafter referred to as AR) are defined as anticyclonic eddies initially detected in the Indian Ocean sector of the domain, and entering the Atlantic Ocean by crossing an imaginary line connecting specific topographic structures (the Protea, Simpson, Wyandot, Schmit-Ott seamounts, and the Agulhas Ridge) that define the southeastern limit of the Cape Basin, southwest of Africa. This line (marked with the letter *C* in Figure 10a) extends from the southern tip of Africa (Cape Agulhas, 35°S and 20°E) to 45°S and 5°E at the southern limit of the Agulhas Ridge in the Southern Ocean. This definition of AR assumes that it is possible to track these eddies and their origin and fate in order to identify them carefully. This identification is carried out for the entire ADT time series. However, in this work, we focus only on AR properties during the period 1 January 2000 to 31 December 2016 to ensure that all AR detected during this period can be tracked back to their origins. Indeed, as we will see later in this section, AR have a particular long life span and can take years to cross the Indo-Atlantic domain.

In what follows, to describe eddy trajectories that include eddy merging and splitting, the concept of *segment network* and *main trajectories* introduced in section 2 are used. The 32,080 anticyclonic eddies that cluster in 122 main trajectories (i.e., order 0 trajectories) are identified as AR entering the South Atlantic from the Indian Ocean. It is then possible to recover the entire network of segments associated with these main trajectories by identifying higher-order trajectories that are linked to the main trajectories by additional merging and splitting events. The total AR network consists of secondary trajectories up to order 29, combining a total of 730,481 anticyclonic eddies and 6,363 segments.

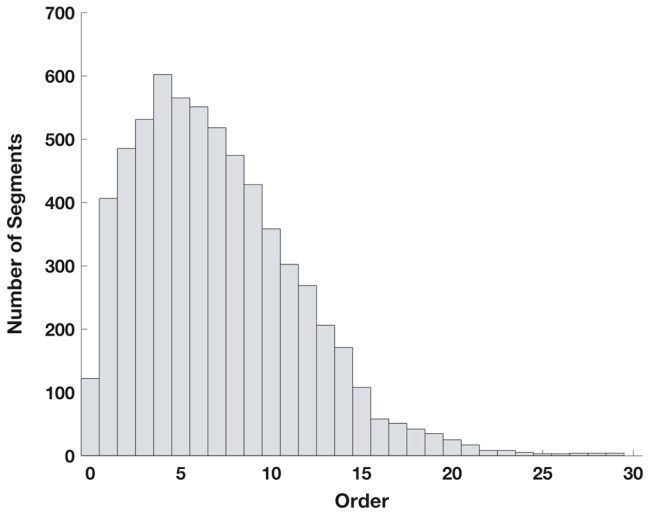

Figure 9. Number of trajectories according to their order associated with Agulhas Rings.

The distribution of AR trajectories according to their order is shown in Figure 9. The distribution is characterized by an increase in the number of segments as a function of trajectory order, from order 0 to the peak corresponding to order 4. Then, the number of new higher-order trajectories associated with AR reduces gradually. The median order of the AR trajectories is 6.

The whole set of AR trajectories (from order 0 to order 29) is presented in Figure 10a, while Figure 10b shows the percentage of time during which each $2° \times 2°$ grid cell is inside an anticyclonic eddy connected to the AR trajectory network. The corresponding figures for order 0, 1 to 4, 5 to 10, 11 to 20, and 21 to 29 are provided in Figures S1 – S5 in the supporting information as well as that of the 19,302 trajectories (1,397,533 eddies) that do not interact with the AR network. In the following, we will refer to the eddies of the AR network as the AR Eddy Network (AREN), which clusters the main AR trajectories (i.e., order 0) and all the additional eddies associated with them via eddy merging and splitting until the maximum order found (29).

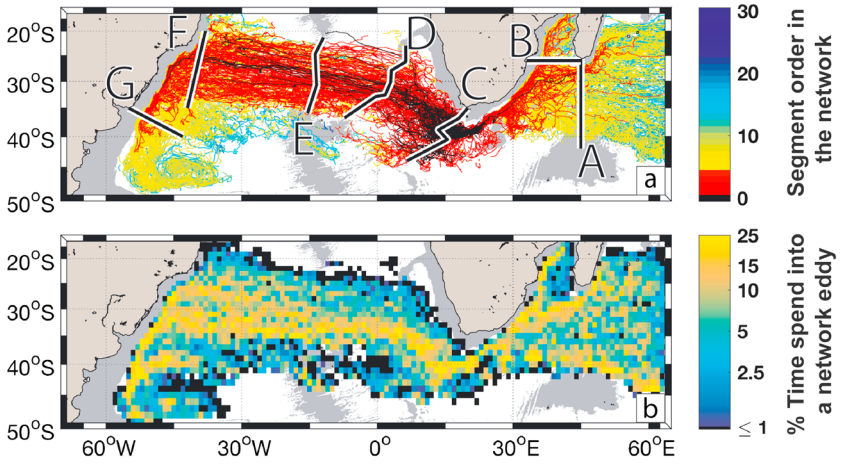

Figure 10. (a) Whole set of Agulhas Ring Eddy Network trajectories (from order 0 to maximum order 29). The color of the trajectories is related to their order. The black color is for order 0, which we defined as the main trajectories for the Agulhas Rings. Seven sections (A–G) were used to derive the Agulhas Rings properties across the basins. (b) Percentage of time each 1° × 1° grid cell is within an Agulhas Ring Eddy Network trajectory. The gray shading in each figure represents water depths less than 3,500 m in the ETOPO2 data set (Smith & Sandwell, 1997).

Figure 10a shows how TOEddies provides a very different overview of the origins, pathways, and fate of AR. Indeed, although the *main* AR trajectories (in black in Figure 10a and in supporting information Figure S1) are relatively similar to the results of the published studies (e.g., Chelton et al., 2011; Dencausse et al., 2010a; Souza, De Boyer Montegut, & Le Traon, 2011), most of them are lost in the Cape Basin or associated with other higher-order trajectories. However, those crossing the South Atlantic basin may be directly related to AR and their region of formation, whereas in previous studies (e.g., Arhan et al., 1999; Byrne et al., 1995; Souza, de Boyer Montégut, Cabanes, & Klein, 2011) this connection could not be made via an objective tracking algorithm because the first detections were found mostly in the Cape Basin, far downstream from the Agulhas Retroflection. This is due to the strength of the TOEddies algorithm, which allows eddies to merge and split and to soundly connect a more complex eddy structure into a main trajectory instead of dealing only with single and well-separated eddies. In addition, the complete set of AREN trajectories (Figure 10a) shows a much richer diversity in terms of origins and fate of AR, and this for AREN trajectories of order 4 or even less (red trajectories in the figure). The resulting AREN trajectories suggest that the eddies contributing to the formation of AR may originate from the southwestern tropical Indian Ocean, further upstream than the Agulhas Retroflection. Figure 10a shows that one AR main trajectory connects directly to the area south of Madagascar. Moreover, AREN trajectories reach regions further downstream than the Cape Basin or the Mid-Atlantic Ridge in the South Atlantic. Indeed, AREN trajectories of orders 1–4 reach the southern end of the South Brazil Current. In particular, two AREN trajectories of order 0 veer south along the South American slope. Furthermore, AREN trajectories of higher order penetrate the Zapiola gyre. The AR trajectories estimated by TOEddies show a clear eddy pathway linking the western boundaries currents of the Indian and Atlantic Oceans.

The main routes undertaken by AREN trajectories are clearly shown in Figure 10b. Three main routes associate Indian Ocean anticyclones to AR: one follows the western boundary slope in the Mozambique Channel, another the slope at the southeastern tip of Madagascar, and the third follows the Agulhas Return Current. The first two seem to merge north of the Agulhas Plateau, around 32°S and 25°E, where the Agulhas Current and the Agulhas Return Current flow in a very narrow corridor between the African slope and this plateau. West of the Agulhas Retroflection (i.e., west of line C in Figure 10a), the AREN trajectories follow, in the Cape Basin, a broad northwesterly route toward a more zonal direction (along the 35°S parallel) once the eddies leave this basin and enter the South Atlantic. At the Mid-Atlantic Ridge, the AREN main path widens until reaching the South American slope between 25°S and 35°S. This wide route in the western part of the South Atlantic seems to consist essentially of trajectories from order 0 to order 4 (Figures 10a, S2, and S3). Once they reach the South American boundary, most eddies head south with the South Brazil Current. However, some trajectories turn north along the western boundary and cross the Cruzeiro do Sul and Vitoria-Trindade seamounts.

Table 3
Properties of the Agulhas Ring Eddy Network Throughout the Geographical Domain

Segment of control	Number of segments	R_{out} (km) median ± STD	Amplitude (m) median ± STD	R_{Vmax} (km) median ± STD	V_{max} (m/s) median ± STD
A: SW Indian Ocean	191	78 ± 43	0.08 ± 0.11	60 ± 35	0.22 ± 0.16
B: Mozambique Channel	30	94 ± 38	0.13 ± 0.14	66 ± 29	0.40 ± 0.17
C: SE Cape Basin	119	81 ± 38	0.21 ± 0.21	65 ± 30	0.47 ± 0.23
D: Walvis Ridge	160	91 ± 39	0.08 ± 0.09	58 ± 22	0.18 ± 0.11
E: Mid-Atlantic Ridge	167	87 ± 42	0.05 ± 0.06	64 ± 27	0.12 ± 0.07
F: S. American Slope	217	74 ± 33	0.04 ± 0.03	57 ± 27	0.12 ± 0.04
G: S. Brazil Current	71	88 ± 41	0.13 ± 0.11	74 ± 37	0.29 ± 0.12

Note. The values are computed at the lines (A–G) plotted in Figure 10a. For each variable, estimates of the median and standard deviation (STD) are provided.

4.2. Characteristics of the Agulhas Rings Network of Trajectories

Although satellite altimetry gives access to ADT 2-D time series, it does not directly infer the 3-D properties of eddies. However, altimetry provides sufficient information to characterize the kinematic and dynamical behavior of eddies, at least in their surface expression and as long as the eddies are detectable from the satellite field. In particular, the TOEddies method gives access to information on horizontal eddy extent (R_{out} and R_{Vmax}), amplitude, azimuthal velocity, and propagation speed. The geographical distribution of the median of these properties is presented in Figures 11 and 12. More precise estimates of these variables are provided in Table 3 at fixed locations. Eddy merging and splitting lead to complex trajectories that can be independent for short periods of time. This highly complicates the description of eddies and their fate in terms of classical eddy trajectories. Indeed, an AR can be associated with many different trajectories because, during its lifetime, it splits in small eddies and eventually merges with other eddies (which can be either AR or anticyclones of different origins). Therefore, we decided to describe the fate of AR by counting the AREN trajectories only when they cross particular sections (lines A–G in Figure 10a). In Table 3 the characteristics of the AREN trajectories across the basin are summarized (in terms of the median and standard deviation of various properties calculated for the geographical lines A to G in Figure 10a). The contributions of the five groups of different AREN trajectory orders (0, 1–4, 5–11, 12–20, and 21–29) to the total number of AREN trajectories crossing the control sections are presented as a percentage in Table 4.

The number of segments entering the Cape Basin since 2000 is 119. This number of segments varies across the domain due to the numerous eddy-eddy interactions and the disappearance of eddies from altimetry maps. The AREN median radii, R_{out} and R_{Vmax}, are relatively constant throughout the domain (see Table 3 and Figure 11a). The medians (±1 standard deviation) R_{out} and R_{Vmax} are 79 km (± 38 km) and 59 km (± 29 km), respectively. The estimate of R_{Vmax} in the Cape Basin, where most AR are documented in the literature, ranges from 58 to 65 km, which are values close to the lower limit of the 65- to 100-km range derived from in situ observations in the Cape Basin by Garzoli et al. (1999) and Arhan et al. (1999). The median amplitude and the azimuthal speed of the AREN are maximum (21 cm and 47 cm/s, respectively) when entering the Cape Basin. Since R_{Vmax} does not vary significantly across the entire domain (Figure 11a), the median of the eddy

Table 4
Distribution of the Orders of the Agulhas Ring Eddy Network Expressed as Percentage When They Cross the Lines (A–G) Plotted in Figure 10a

Segments of control	Order 0 (%)	Orders 1 to 4 (%)	Orders 5 to 10 (%)	Orders 11 to 20 (%)	Orders 21 to 29 (%)
A: Southwest Indian Ocean	1	9	66	22	2
B: Mozambique Channel	0	27	60	13	0
C: Southeastern Cape Basin	100	0	0	0	0
D: Walvis Ridge	12	80	8	0	0
E: Mid-Atlantic Ridge	7	75	16	2	0
F: South American Slope	2	44	52	2	0
G: Southern Brazil Current	0	13	80	7	0

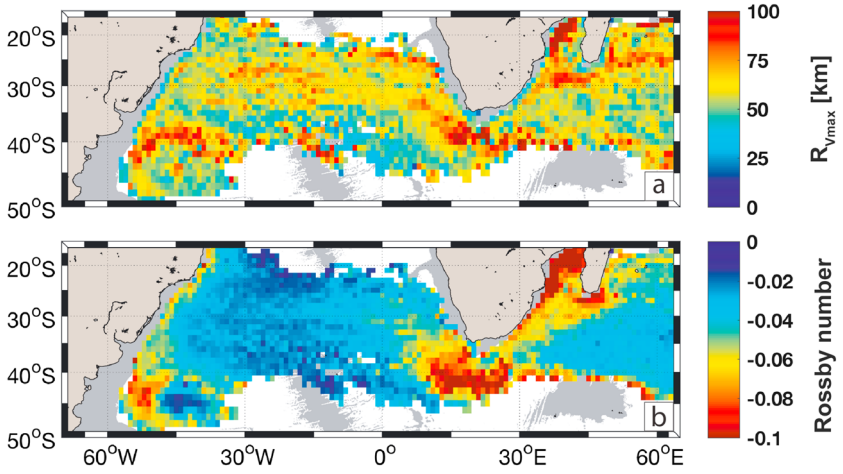

Figure 11. (a) Median of Rossby number (Ro) and of the (b) equivalent radius of the characteristic contour (R_{Vmax}) of the Agulhas Ring Eddies Network. These properties are computed on a 1° × 1° grid. The gray shading in each figure represents water depth shallower than 3,500 m in the ETOPO2 data set (Smith & Sandwell, 1997).

vortex Rossby Radius, Ro, (Figure 11b) provides an indirect measure of changes in eddy azimuthal velocity. This velocity is highest in the Agulhas Current System and in the southern half of the Cape Basin and from there it decreases rapidly and remains constant across the South Atlantic Ocean. It is only when the AREN trajectories reach the South American boundary that Ro increases again, most likely due to the interactions of eddies with the South Brazil Current and local anticyclones.

In addition to the inherent properties of the AREN eddies, it is interesting to evaluate their median propagation speed (Figure 12), as it can be used to estimate their transit time through the different zones. The regions where AREN eddies move faster correspond to the western boundary currents (WBCs) of the Indian Ocean and also of the South Atlantic (reaching speeds higher than 0.1 m/s). The AREN propagation speed remains high in the Cape Basin (although it is higher in the Southern than in the Northern Cape Basin) and in the South Atlantic, especially for the northern sector of the route, west of the Mid-Atlantic Ridge. The AREN direction of propagation (Figure 12b) clearly shows different regimes of fast southwestward flow in the WBCs, northwestward flow in the Cape Basin, and westward flow in the South Atlantic. It also shows that the AREN path along the Agulhas Return Current involves eddies moving eastward. These eddies are most likely related to AR as

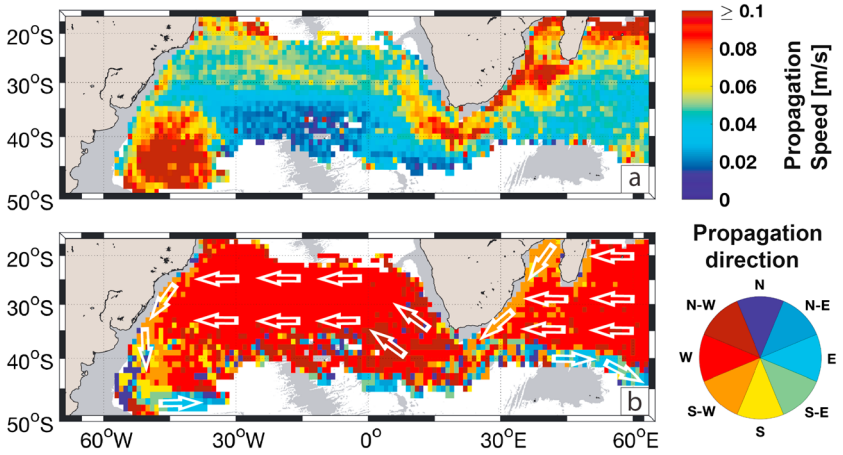

Figure 12. (a) Median of the propagation velocity of the Agulhas Ring Eddy Network (m/s) and (b) associated main propagation direction. These properties are calculated on a 1° × 1° grid, and the propagation direction is computed from the eddy positions 1 week apart. Schematic white arrows have been added in the bottom panel to highlight the main propagation direction. The gray shading in each figure represents water depth shallower than 3,500 m in the ETOPO2 data set (Smith & Sandwell, 1997).

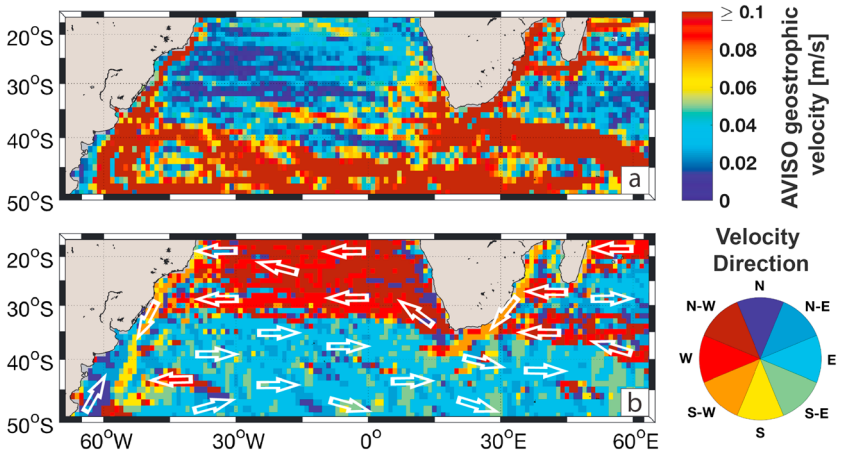

Figure 13. (a) Mean surface geostrophic velocity estimated from AVISO satellite altimetry (m/s) and (b) associated main direction. These properties are computed on a 1° × 1° grid. Schematic white arrows have been added in the bottom panel to highlight the main velocity direction. The gray shading in each figure represents water depth less than 3,500 m in the ETOPO2 data set (Smith & Sandwell, 1997).

a product of AR splitting in the Agulhas Retroflection area, which are successively advected eastward in the intense Agulhas Return Current.

To better characterize the kinematics and dynamics of the AREN eddies, their median propagation velocity can be compared with the mean surface geostrophic velocity estimated from AVISO satellite altimetry (Figure 13). The AREN and AVISO estimates of velocity intensities compare relatively well in terms of propagation direction with the mean surface velocity in the WBCs and the Agulhas Return Current with, in general and, as expected, the AREN propagation speed being an order of magnitude less than the surface geostrophic velocity. Here the eddies are advected with the mean current. However, differences between AVISO and AREN mean velocities occur in the northern subtropical South Atlantic where eddies appear to move westward at a higher velocity (about 6 cm/s) than the mean surface geostrophic velocity (about 2 to 4 cm/s), and in the southern subtropical Atlantic (south of 30°S) where they move westward against the mean surface current (which flows eastward as expected for the poleward branch of the South Atlantic gyre; see Figures 12, 13, and 1b). The ratio of the AREN translation speed and the mean geostrophic current are computed in each 1° × 1° grid cell (Figure S7 in the supporting information). It shows that AREN move faster than the mean surface gesotrophic current in 60% of these cells.

McDonagh et al. (1999) studied the mechanisms responsible for the translation of Agulhas Rings in the Cape Basin. They showed from two specific AR that the self-advection mechanism (Cushman-Roisin et al., 1990; Rhines, 1975) is not sufficient and conclude that the main factor appears to be the advection by the main flow. These results are consistent with our findings that high AREN translation values are found where geostrophic surface velocities are also important. This is verified in the WBCs and in the Cape Basin. However, in the South Atlantic, AREN eddies move faster, if not against the surface geostrophic flow. Here, most likely, the main mechanism of translation is the self-advection of eddies.

4.3. Agulhas Rings Origins, Disappearance, Splitting, and Merging

To better describe the AREN, we discuss here the statistics in the regions where they are initially identified, where they disappear as well as the distribution of eddy merging and splitting events. The description of AR as anticyclonic eddies participating in the AREN may not be appropriate because they are associated with a large number of eddy merging and splitting events (i.e., high-order trajectories). For this reason, we put a particular emphasis on estimates of AREN trajectories up to order 4, which correspond to the peak of the number of trajectories as a function of the trajectory order (Figure 9). In the following, we will call this subgroup of AREN, AREN4.

The distribution of eddy formation, disappearance, and merging and splitting within AREN4 is presented in Figure 14 and that of the total AREN in Figure 15. To better assess the regionalization of these processes, only the 2° × 2° cells showing more than 5 (10) or 10 (10) first/last detections (merging/splitting) events for AREN4 and AREN, respectively, are presented. The difference in threshold used for the two different types of

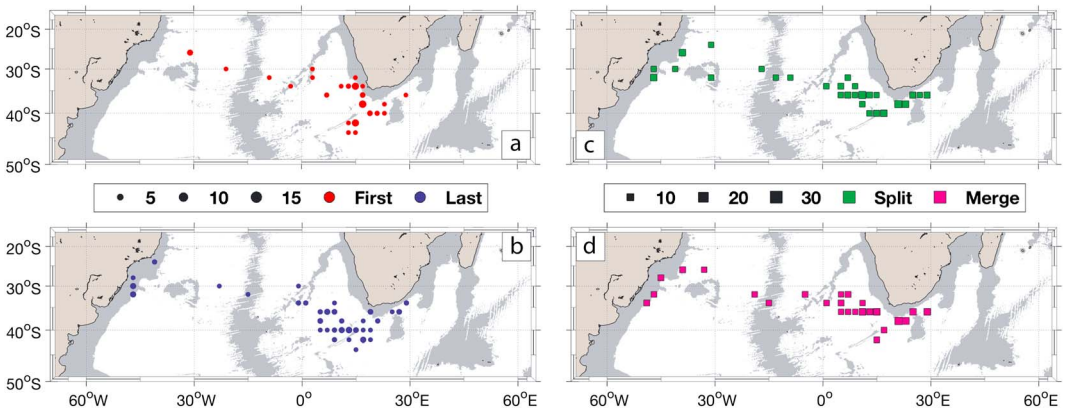

Figure 14. The 2° × 2° gridded positions and number of first detections (a), last detections (b), merging events (c), and splitting events (d) of the AREN4 (i.e., AREN with orders less than 4). Each dot size represents the number of events for each grid cell associated with more than 10 occurrences. The gray shading in each figure represents water depth shallower than 3,500 m in the ETOPO2 data set (Smith & Sandwell, 1997). AREN = Agulhas Ring Eddy Network.

events is explained by the fact that TOEddies records approximately twice as many trajectory interactions as eddy formation or disappearance events. One hundred nineteen AREN cross, flowing west, line C in Figure 10 (Table 3). This line defines the AR trajectories, which explains why only zeroth-order eddies enter the Cape Basin (Table 4). Most AR are initially identified at the Agulhas Retroflection as shown by the large red patches near the Cape Basin in Figure 14a and the starting points of the black and red trajectories in Figure 10a. This region extends over a large area, between the Agulhas Bank, the Agulhas Plateau, and the Agulhas Ridge, and agrees with the entire Agulhas Retroflection position, from 8°E to 25° – 28°E (e.g., Dencausse et al., 2010b; Lutjeharms & Ballegooyen, 1988).

In addition to this traditional view of AR shedding from the Agulhas Current at the Agulhas Retroflection, our method identifies anticyclonic eddies formed at the southern edge of the Agulhas Return Current as previously observed by Lutjeharms and Ballegooyen (1988) and Boebel, Rossby, et al. (2003). Indeed, some eddies can merge with or split from a newly shed AR, which is why we classify them as AREN. Many new AREN4 are located near the African continent in the northeastern part of the Cape Basin. Other locations of AREN4 origins appear near the Walvis Ridge and further west the South Atlantic. These areas of eddy formation may be related to splitting of AREN4 eddies or to the merging of eddies of distinct origins with AREN4 trajectories.

Moreover,113 of the 888 anticyclonic eddies that start an AREN4 trajectory are east of 30°E. Taking into account the AREN as a whole (Figure 15), the results suggest that a relatively small number of AREN4 originate as far north as the Mozambique Channel or east of the Madagascar Ridge while many higher-order AREN

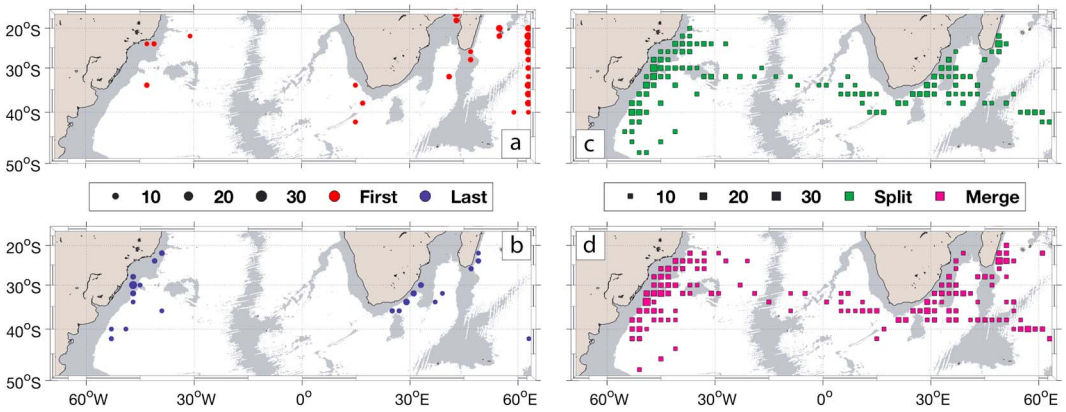

Figure 15. The 2° × 2° gridded positions and number of first detections (a), last detections (b), merging events (c), and splitting events (d) of the Agulhas Ring Eddy Network. Each dot size represents the number of events for each grid cell associated with more than 10 occurrences. The gray shading in each figure represents water depth shallower than 3,500 m in the ETOPO2 data set (Smith & Sandwell, 1997).

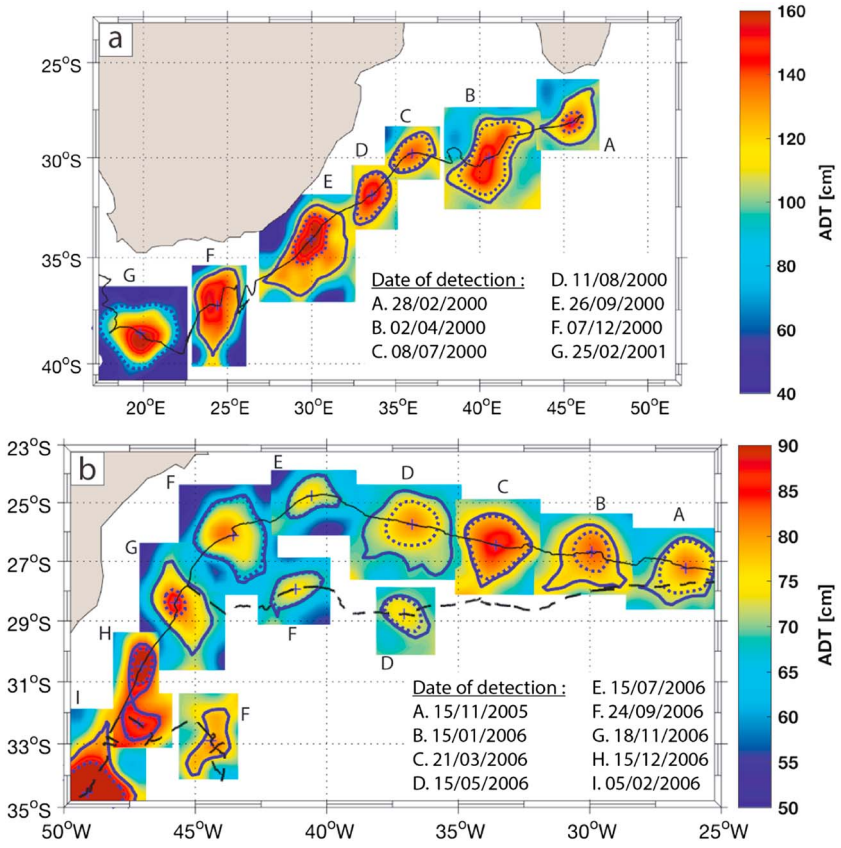

Figure 16. Composite figure of the order 0 Agulhas Ring Eddy Network starting the most to the east (a) and ending the most to the west (b). Snapshots on selected dates are given, in blue the eddy centroid (cross symbol), the absolute dynamic topography (ADT) contour associated with the maximum speed (dotted), and the outermost ADT (solid line) contours. The trajectory of panel (b) interacts with two order 1 trajectories whose paths are drawn in dashed lines.

trajectories are as it appears from Table 4. Only one third of the AREN trajectories formed in the Mozambique Channel are reconstructed taking into account trajectories of order 4 or less, whereas 90% of the trajectories originating in the Southwest Indian Ocean are obtained by taking into account trajectories at orders greater than 4. Figure 10b, which highlights the area where many AREN eddies are present over the period of interest, shows a clear link between these northeast formation regions and the Agulhas Retroflection. This pattern is very similar to the many large eddies detected from surface drifters documented by Zheng et al. (2015) .

The existence of these anticyclones and their possible role in the destabilization of the Agulhas Current, leading to meanders, have already been documented (e.g., Biastoch, Böning, & Lutjeharms, 2008; Biastoch, Lutjeharms, et al., 2008; Elipot & Beal, 2015; Halo et al., 2014; Penven et al., 2006; Schouten et al., 2002). Schouten et al. (2002) also found that some of these eddies do not create meanders and are advected downstream to the Retroflection. Detections of these eddies could be associated with an artificial interruption of the Agulhas Current due to the interpolation used to estimate the gridded altimetry field from the altimeters along-track data. However, the amplitude of these eddies is greater than 10 cm near the Agulhas Current. Therefore, they appear to be well-defined structures and not an artifact of data interpolation. A composite view of the zeroth-order trajectory that originates from the southern tip of Madagascar is shown in Figure 16a. This eddy forms near Madagascar and remains very coherent until it reaches the Cape Basin. Furthermore, this type of eddies is also well captured by looping drifters (Lumpkin, 2016; Zheng et al., 2015) and the in situ data recorded by current meter moorings (Donohue et al., 2000). Many new detections of AREN eddies are also occurring in the open Indian ocean, which corresponds to the eastern part of our domain of study. In particular, Reunion Island, southeast of Madagascar, seems to be an active region for the identification of new AREN eddies. In summary, our results suggest that AR can form upstream of the Agulhas Retroflection and move relatively rapidly southward with the Agulhas Current (Figure 10d) until they are blocked between the Agulhas Current and its Return Current in the Retroflection area where they may merge with another eddy or be shed.

While AR origins have often been discussed in the literature, although not in the more complex context of the AREN, their disappearance has not yet been examined thoroughly. The TOEddies method and the AREN approach make it possible to quantitatively infer the vanishing of AR from satellite altimetry maps. Figure 14b documents a very well structured pattern for the main regions where TOEddies lose the AREN4 ADT signature. This occurs mainly in the Cape Basin, not far from the main source regions of AREN4. This suggests that most AREN4 trajectories are lost within the Cape Basin, relatively soon after entering the region. The general pattern of disappearance of AREN4 is not evenly distributed: Most eddies disappear in the southern half of the basin as well as near the Walvis Ridge. Other regions where AREN4 vanish from ADT maps are found north of the Agulhas Plateau, south of Africa, and near the South American slope. There is no appearance or disappearance of AR, within AREN4, in the open ocean in the South Atlantic except occasionally.

According to the TOEddies method, there are more merging and splitting events than appearance and disappearance. The recurrence of such eddy-eddy interactions in the Retroflection area and in the Cape Basin has been demonstrated by various authors from in situ and remote sensing data (Arhan et al., 1999; Baker-Yeboah et al., 2010; Boebel, Lutjeharms, et al., 2003; Byrne et al., 1995; Dencausse et al., 2010a). Our study shows that these regions correspond to areas where these processes are particularly active (Figures 14b and 14c). Topographic features are also regions where many merging and splitting events occur.

To complete the description of AR behavior in the South Atlantic, we discuss in the following sections the AREN regional behavior and statistics in more detail.

4.4. Agulhas Rings in the Cape Basin

Taking into account our definition of AR (anticyclones leaving the Indian Ocean and entering the Cape Basin, Figure 10a), we have identified 119 AREN4 (see Table 3). This is equivalent to a rate of seven AR entering the Cape Basin per year. This represents a higher ratio than previous estimates that typically suggested one event every 2 to 3 months (e.g., Gordon & Haxby, 1990; Goni et al., 1997; Schouten et al., 2002). However, some authors (Baker-Yeboah et al., 2010; Dencausse et al., 2010a; Schouten et al., 2000) suggested that AR often split shortly after their shedding from the Agulhas Retroflection, before entering the Cape Basin. This may explain why our estimate is higher than those provided in previous studies that did account for splitting events. Indeed, eddy splitting and merging are particularly abundant near the Retroflection area (Figure 14c).

Looking separately at newly formed AR and those resulting from a splitting, we find a mean value of 4.3/year for newly formed AR entering the Cape Basin (i.e., a total of 73), while 2.8/year results from a splitting. Thus, about two thirds of the AR entering the Cape Basin are newly formed and the remainder result from a splitting. These results are very similar to those of Dencausse et al. (2010a) although their estimate is twice as high. To conclude, on average, every 2.8 months, a newly formed AR enters the Cape Basin. This rate is very similar to those found in the literature in terms of AR shedding (e.g., Goni et al., 1997; Gordon & Haxby, 1990; Schouten et al., 2002).

At the Agulhas Retroflection and in the southern Cape Basin, the AREN trajectories are essentially made by AREN4 (i.e., rows C and D in Table 4 and Figures S1 to S5 in the supporting information). Here AREN are characterized by large Ro (Figure 11a) in the area where they are mainly spawned (Figure 14a and line C in Table 3). A sudden transition in Ro appears when AR enter the Cape Basin (Figures 10b and 11a). This transition is due to a decrease in AR surface V_{max} and amplitude (and thus surface vorticity), whereas the radii remain relatively constant (Table 3). A decrease in vorticity in the Cape Basin has already been observed although not quantitatively documented (e.g., van Sebille et al., 2010).

Eddies in the Cape Basin have a particularly complex behavior that has been suggested by previous studies (e.g., Arhan et al., 1999; Boebel, Lutjeharms, et al., 2003; Dencausse et al., 2010a; Schouten et al., 2000). Here we can try to characterize this type of behavior more extensively. As already mentioned, TOEddies takes into account numerous AR separations and coalescences throughout the Cape Basin (Figures 14c and 14d). Although Figure 14b shows a main path of AR to the northwest suggesting straight trajectories, their individual behavior is truly complex due to eddy-eddy interactions and induces relatively long residence times. The real impossibility of associating a trajectory with a single eddy but rather the need to consider the full set of AREN trajectories complicates the definition of a mean residence time associated with AR for each specific region of the domain considered. We propose here to overcome this difficulty by considering all the AREN trajectories reconstructed from each segment crossing each line in Figure 10a. In this way, we can estimate the residence time of the AREN eddies in the Cape Basin by considering the segments that cross the Walvis Ridge (i.e., line D in Figure 10a) and that are associated (backward in time) with segments that cross the southeast

limit of the Cape Basin (i.e., line C in the Figure 10a). We limit the reconstruction of the network to trajectories of order 15.

One hundred of the 119 AREN4 trajectories crossing line C are associated with a median order of 2 (i.e., 2 eddy-eddy interactions that include eddy splitting and merging). Based on these trajectories, we find that the mean residence time of AR in the Cape Basin is about 1 year (median of 1.0 ± 0.5 years), which corresponds to the estimate of Schouten et al. (2000). During their journey in the Cape Basin, AR undergo important changes affecting their surface signature, as shown in Figures 11 and 12 and Table 3 in terms of several dynamical and kinematic properties. In particular, although their sizes remain relatively stable, their initial surface signatures in amplitude, Ro and V_{max} decrease by ~50% on average.

While 119 AREN4 enter the Cape Basin, 160 cross the Walvis Ridge and enter the South Atlantic (Table 4). Again, because TOEddies does not associate a trajectory with a single eddy, these two values cannot be linked directly. Indeed, the number of eddy splitting and merging events in the Cape Basin is very high (Figure 14c) as is the number of eddy disappearances. In particular, Figure 14b shows that many of the initial 119 AR are lost on satellite altimetry maps in the southern Cape Basin.

4.5. Agulhas Rings Across the South Atlantic

The fate of the 119 AREN4 that cross the Walvis Ridge and enter the South Atlantic Basin appears more linear and less turbulent than in the Cape Basin. They flow in a very zonal direction (centered around 35°S and about 5° wide). Here their disappearance from the altimetry maps is almost nil (Figure 14b for AREN4 and Figure 15b for the whole AREN). The number of merging and splitting events is also significantly reduced. The main area where eddy-eddy interactions become important again corresponds to the Rio Grand Rise in the western part of the South Atlantic while the Mid-Atlantic ridge is not associated with such events but has an impact on the AREN zonal route by increasing its width (which becomes 10° wide).

A large portion of the AREN4 crossing the Walvis Ridge reaches the Mid-Atlantic Ridge (line E in Figure 10a), which represent 82% of the AREN passing this ridge. The very coherent behavior of the AREN crossing the South Atlantic is well captured by reconstructing the network and crossing times between lines E and D. On average, AREN eddies cross the eastern South Atlantic in about 1 year (a median time of 1.0 ± 0.3 years) with a median of only 1 eddy-eddy interaction. However, the AREN behavior changes on the other side of the Mid-Atlantic Ridge. Here the contribution of AREN4 to AREN reaching the South American slope is only 46%. This may be the result of the numerous eddy-eddy interactions at the Rio Grand Rise that has an impact on the overall behavior of the trajectories. The western part of the South Atlantic is crossed in 1.5 years (a median value of 1.5 ± 0.6 years computed between lines E and F) with a median of three eddy-eddy interactions.

Finally, Figure 10c shows a clear decrease in the surface intensity (Ro) of AREN eddies across the South Atlantic, associated with a 43% decrease in their surface azimuthal velocity V_{max} and 60% in their amplitude, while their size remains relatively stable (from lines D to F in Table 3).

Many authors (e.g., Byrne et al., 1995; Gordon & Haxby, 1990; Schouten et al., 2000) have demonstrated the ability of AR to penetrate the South Atlantic Ocean, claiming that they gradually dissipate and vanish in this basin. Our study suggests a different fate for these eddies since nearly half of the AREN4 reaches the South American continent. Among these trajectories, 4 are order 0 AREN.

4.6. Agulhas Rings Along the South American Margin

Despite their relatively low surface signature, the few AREN eddies that are still detectable by satellite altimetry and that reach the American slope maintain their coherence. Near the South-American coast, they propagate southward in the South Brazil Current (Figure 10) for about half of a year (0.9 ± 0.5), as suggested by Byrne et al. (1995). Along this path, AREN eddies undergo numerous eddy-eddy interactions as indicated by the large number of merging and splitting events (Figure 15b). These interactions are characterized by a sudden increase in surface signature and propagation speed (Figures 11 and 12). Moreover, some newly formed anticyclonic eddies are identified as AREN when they merge with older structures. A composite view of the trajectory at 0 order that ends further west is shown in Figure 16a. This AR veers south when it reaches the South American coast. There another anticyclonic eddy merges with it in October 2006. Two months later, the trajectory of order 0 merges with a newly formed anticyclone which results in the formation of an intense and large anticyclone.

At the southern limit of the Brazil Current and in the Zapiola Gyre, AREN eddies show an intense surface signature, as high as in the Cape Basin, before their trace is gradually lost. However, assessing the effective con-

tribution of the original AR to these long trajectories remains a challenge due to the numerous merging and splitting events that occurred during their lifetime, and, in particular, along the Brazilian continental slope.

5. Summary and Conclusions

In this study, we present TOEddies, a new eddy identification and tracking algorithm that takes into account the detection of eddy splitting and merging events which has been applied to gridded multisatellite ADT maps. Because of the many eddy-eddy interactions and the resulting eddy subdivisions and coalescences, the concept of a trajectory associated with a single eddy becomes less obvious than previously admitted. However, to be able to track the origins, fate and changes of these eddies we have reconstructed a network of segments and trajectories that allow us to reconstruct the history of the eddies.

We also developed a method to objectively assess the robustness and skill of TOEddies against loopers, an eddy atlas derived from the completely independent set of drifting buoy data (Lumpkin, 2016). This allowed us to quantitatively compare and test TOEddies against the eddy atlas distributed by SSALTO/DUACS (Duacs/AVISO+, 2017). TOEddies proved to be more robust because the eddies it detects correspond better (by 10% and with a smaller error) to those identified from surface drifter data.

After validation, this algorithm was applied to daily AVISO ADT maps from 1993 to mid-2017 to uncover and characterize quantitatively the dynamics of Agulhas Rings entering the South Atlantic Ocean. After the complete recovery of the trajectories, the eddy statistics from January 2000 to December 2016 were explored. To differentiate with the stricto sensu definition of Agulhas Rings formed in the Indian Ocean and disappearing in the South Atlantic, we used the concept of trajectory networks to define the AREN.

The characteristics of the AREN, such as their surface signature and propagation speed near the Agulhas Retroflection, compare particularly well with previous estimates produced for a limited number of structures (e.g., Arhan et al., 1999; Dencausse et al., 2010a; Garzoli et al., 1999; ; Gordon & Haxby, 1990; Schouten et al., 2002). However, our study contradicts the traditional view of large coherent Agulhas Rings shed at the Agulhas Retroflection that are propagating and dissipating rapidly in the South Atlantic Ocean. For example, our results suggest that Agulhas Rings, and other anticyclonic eddies connected via merging and splitting, may originate as far upstream from the Agulhas Retroflection as in the Mozambique Channel or South of Madagascar. From there, they are advected southward by the Agulhas Current as distinct coherent structures without being absorbed or dissipated by the current.

Throughout their existence, Agulhas Rings interact intensely with neighboring eddies, giving rise to very complex trajectories. These interactions are particularly vigorous in the Cape Basin and influence the time these eddies spend in the region which is, on average, relatively long (about 1 year). Here they undergo major changes in their surface properties (dynamic height and azimuthal velocity), while their lateral size remains relatively constant. These changes are likely due to local air-sea, eddy-eddy, and eddy-topography interactions (Arhan et al., 2011, 1999; Dencausse et al., 2010a).

Numerous Agulhas Rings disappear from altimetry maps in the Cape Basin preventing their subsequent tracking. This may be due to their subduction in the ocean interior and not necessarily to eddy dissipation because, in this region, Agulhas Rings release large amounts of heat in the atmosphere and become denser (Arhan et al., 2011). Indeed, evidence of their subduction has been observed by Arhan et al. (1999) and Garzoli et al. (1999). Based on these observations, Herbette et al. (2004) used an idealized numerical simulation to show that the surface signature of such eddies can decrease considerably while they are still propagating in the ocean interior.

The AREN that we can still track in the Southwest Atlantic, follow a quasi-zonal path, about 5° wide along the 35°S parallel, which widens further when passing the Mid-Atlantic Ridge. They eventually reach the South American continental slope where the majority of them propagates southward with the South Brazil Current. Here they often merge with other anticyclones flowing south with the current and originating north of 20°S. Some AREN eddies can be detected along the western slope of the South Atlantic as far south as the Zapiola gyre.

Our results suggest that Agulhas Rings can live longer than expected. The longest main (i.e., 0 order AREN) trajectory is more than 4 years old, whereas, if we compute the travel time of the network through lines C to

G, we find a median time of 5 years for the trajectories connecting the eddies of the Southeast Indian Ocean to their furthest destination in the Southwest Atlantic.

Our study reveals a different view of the Agulhas Rings from that provided in previous studies. However, it does not necessarily disagree with their conclusions. Indeed, TOEddies is able to reconstruct a longer and more complete history of these eddies that encompasses the various Agulhas Rings segments of trajectories discussed in the literature.

The most important outcome of our study is probably the assessment of numerous eddy splitting and merging events involving Agulhas Rings and also anticyclonic eddies of different origins, which leads to the formulation of the AREN. This is essential for a better understanding of ocean dynamics. Indeed, eddy separations and coalescences must induce a vigorous mixing of water masses advected in the core of the eddies, which has an important impact on the overall redistribution of the physical and biogeochemical water properties. As suggested by Wang et al. (2015), Agulhas Rings cannot be considered as coherent and isolated structures advecting the same water masses along their path. Therefore, our results provide a different perspective on eddies from most published studies that do not account for eddy separations and merging events (e.g., Chelton et al., 2011; Faghmous et al., 2015; Haller & Beron-Vera, 2013). However, if TOEddies can deduce the surface signature of eddies, it is still limited because it cannot access the exact processes involved in the evolution of eddies nor their subsurface structure.

Agulhas leakage plays an important role in the climate system, as a mechanism for transporting heat and salt between basins and closing the large-scale overturning circulation (Beal et al., 2011; Gordon, 1985). In the context of global warming and early evidences of a changing Agulhas Current system and leakage (Beal & Elipot, 2016; Biastoch, Böning, & Lutjeharms, 2008; Rouault et al., 2009) our results highlight the role of Agulhas Rings as an important, albeit complex, vector for Indo-Atlantic exchange. They reveal a new long route for these eddies, unequivocally connecting the WBCs of the Indian and South Atlantic oceans.

However, although modeling studies using Lagrangian techniques suggest a direct connection between the Agulhas Leakage and the AMOC (Rühs et al., 2013; van Sebille et al., 2011) with more than 50% of the Agulhas Leakage reaching the North Atlantic, our study does not show such a direct link for the Agulhas Rings as most of them recirculate southward with the South Brazil Current. Yet a small number of these eddies appear to veer northward, crossing the Cruzeiro do Sul and the Vitoria-Trindade seamounts chains. These results leave open the question of how the connection between the Agulhas leakage and the AMOC, as seen by the models, is achieved. Is the volume transport of these few eddies north of 20° intense enough to close the AMOC transport budget? Are all these eddies the ones that make the connection or are most of them invisible from altimetry because they flow northward at depth, as subsurface eddies? Finally, do the Agulhas Rings really make the connection with the AMOC or is this achieved by circulating water around the mesoscale field?

Although this study describes a much more complex Agulhas leakage made by Agulhas Rings than previously observed, our results are still incomplete because they cannot go beyond the limits of satellite altimetry. Indeed, altimetry maps are reconstructed from scattered observations that most probably affect the number of objectively recoverable eddies and trajectories. Moreover, these results are limited to the surface description of certain kinematic and dynamic properties. For a more in-depth description of these eddies and a quantitative estimate of the Agulhas leakage, future work should focus both on the variable three-dimensional structure of the Agulhas Rings and understanding all the processes that govern the connection of the Agulhas Current system with the AMOC.

Appendix A : Validation of the TOEddies Method and Parameters

In this appendix, we describe in detail some aspects of the analyses and cross validation presented in the core of the article.

A1. Sensitivity of the Algorithm on the Persistence Parameter

To assess the skill of the method, we developed a systematic procedure that tests the presence and properties of eddies against the loopers, the independent eddy data set derived from surface drifting buoys by Lumpkin (Lumpkin, , LU16 in the following). This was used in the manuscript to infer the efficiency of the algorithm and to compare it to the database distributed by Duacs/AVISO+ (2017) and based on Chelton et al. (2011) method and modified by Schlax and Chelton (2016).

Table A1
Eddy Detection and Collocation Statistics With LU16 Loopers for Four Data Sets for the Persistent Threshold From 0 to 10 mm

Data Set	Number eddies anti/cyclo (10^6)	Sum area max anti/cyclo (10^{10} km^2)	Sum area out anti/cyclo (10^{10} km^2)	Match anti max/out (%)	Mismatch anti max/out (%)	Match cyclo max/out (%)	Mismatch cyclo max/out (%)
ADT_00	3.1/3.2	2.7/2.4	4.1/3.8	63/66	1/2	69/71	1/1
ADT_01	3.2/3.3	3.2/2.8	5.2/4.6	66/71	2/3	71/75	1/2
ADT_05	3.1/3.2	3.1/2.8	5.2/4.6	66/71	2/3	71/75	1/2
ADT_10	2.8/2.9	3.1/2.7	5.2/4.6	66/71	2/3	70/75	1/2

Note. The *max* annotation refers to the eddy contours associated with the maximum eddy azimuthal speed, while the *out* annotation refers to the outer eddy contours. The percentages indicate the fractions of eddies by polarity as defined in LU16. Anti and Cyclo stand for respectively anticyclonic and cyclonic eddies.

This procedure was also used to test the sensitivity of TOEddies to its parameters and their value. These sensitivity studies have shown that the persistence is the most important parameter of the algorithm. This parameter, which prescribes a minimum value as an eddy amplitude threshold, is based on topological simplification studies (Edelsbrunner & Harer, 2010; Edelsbrunner et al., 2002). It is applied to isolate the local extremes of altimetric fields whose value is high enough to be considered robust in terms of signal-to-noise ratio. It can be compared to the minimum amplitude threshold often used in eddy detection algorithms found in the literature (e.g., Chelton et al., 2011). However, while the latter is applied to eddies after they have been identified, the persistence parameter is integral part of the eddy identification step of the TOEddies algorithm because it is used to select the altimetry extremes to be considered as eddies. This is to ensure, for example, the detection of the merging of two or more eddies, or the growth of a large eddy. Indeed, if the algorithm finds in a relatively large area more than one extreme, the TOEddies algorithm automatically identifies more than one eddy because it requires that the eddies should contain one and only one extreme. This is true unless all but one of the extremes have values below the threshold limit. In this case, TOEddies identifies a single large eddy and not two or more.

Four eddy data sets are presented in Table A1 that lists the number of eddies identified by each of them and their detection efficiency expressed as a percentage of the total number of collocations with LU16 eddies. These data sets were created by varying the minimum amplitude threshold (i.e., the persistence) for the identified ADT extremes and are labeled accordingly: ADT_MinPersistenceThreshold. No tracking considerations were applied on them. Hence, ADT_01 corresponds to the ADT_raw data set presented in the core of the article.

This parameter directly influences the number of eddies: when it is not 0, the higher is its value, the lower the number of detected eddies (Table A1). We observed that this parameter has the greatest impact when it goes from a value of 0 to 1 mm, and less for values greater than 1 mm (see rows for ADT_00 and ADT_01 in Table A1). In fact, a nonzero value, as small as 1 mm, for persistence increases the number of eddies detected. This is explained by the fact that it takes at least four grid points for an eddy to be defined as such by the method. When examining the effectiveness of matching TOEddies with LU16 loopers, a value of 1 mm compared to 0 for the persistence parameter increases the matching by up to 8%. For threshold values greater than 1 mm there is no significant increase in the matching.

While a nonzero threshold value for persistence increases the number of detections, as well as the total area occupied by eddies and the efficiency of detecting eddies associated with LU16 loopers, it also increases the number of erroneous detections (computed as the mismatch in polarity between TOEddies and loopers) by a large fraction (up to 50%; see Table A1). These errors increase with the threshold value. However, for a threshold value of 1 mm, they are negligible for eddies larger than 25 km (see Figure 8 in the main text). For these reasons, we chose the threshold value of 1 mm when applying TOEddies to altimetry maps.

A2. Validation of the Eddy Detection Algorithms

The results of the cross validation between LU16 and the different eddy satellite altimetry databases listed in Table 1 are discussed in detail below. Table 2 shows the number of eddies identified in each data set and their detection efficiency expressed as percentages of the total number of collocations with LU16 eddies. To assess the skill of the method and provide quantitative comparisons between the different eddy data sets, a matching percentage is computed. It represents the proportion of each polarity of the LU16 eddies that

were successfully cross detected with eddies of the same polarity in each data set (Table 2). Cross-detection errors are also defined as mismatches in eddy polarity or when several eddies detected by altimetry have been assigned to the same LU16 eddy.

The TOEddies detection algorithm was tested on the SLA and ADT maps (without applying an eddy lifetime threshold) to evaluate the most relevant altimetry data set for automatic eddy detection. Table 2 shows that the TOEddies algorithm (referred to as SLA_raw and ADT_raw) detects 34% (36%) more anticyclonic (cyclonic) eddies when SLA instead of ADT maps are used. The total area occupied by eddies derived from SLA is larger than that resulting from the use of the ADT field. This area is 31% (50%) higher than the surface encompassed by the eddy contour defined by R_{Vmax} for anticyclones (cyclones) and by 48% (65%) when the eddy boundary contour is defined by R_{out}.

When comparing the effectiveness of the results with LU16 and using the outer contour as eddy edge (Table 2), the ADT maps show a slightly better agreement for anticyclones (by about 2%), while the SLA maps give a slightly better result for cyclones (by about 3%). On the other hand, when the contour of maximum velocity is taken as the eddy boundary, the differences in detection efficiency between the SLA and ADT maps decrease in the case of cyclones while, for anticyclones, the ADT shows better results (4% more effective).

To validate the robustness of the TOEddies threshold requiring a minimum longevity of 4 weeks for a trajectory segment, the results of ADT_raw and TOEddies are compared. Table 2 shows that such a threshold reduces both the number and total extent of eddies. The number of eddies decreases by 25% and the total area they occupy by 10%. This is mainly due to the fact that the threshold over the eddy lifespan reduces the number of small eddies. In terms of validation compared to LU16, the number of collocations decreases for both cyclones and anticyclones when the time threshold is used (Table 2). This is particularly true for cyclones. Note here that the highest matching of the algorithm, independent of the time threshold or the altimetry field, is obtained for the eddy perimeters defined by the outer contour although there is a slight increase in errors.

As META2017 is probably the most widely used eddy atlas derived from satellite altimetry, in order to have another independent measure of the performance of our algorithm, we quantitatively compare META2017 and TOEddies overall statistics and skills. Table 2 suggests that META2017 identify 25% fewer eddies but their overall extent is 41% larger. Figure 7 shows the statistical distribution of META2017 and TOEddies radii. The distribution maximum is positioned at about 40 km for TOEddies and 60 km for META2017. A clear difference between cyclones and anticyclones appears in TOEddies where cyclones are, on average, smaller than anticyclones. This difference is also noticeable in META2017, but less marked. In TOEddies, fewer than 1% of the eddies have a radius greater than 140 km, while it corresponds to 5% of the structures for META2017.

To compare the size of eddies detected by satellite altimetry with an independent variable related to mesoscale ocean dynamics, we estimated the first Rossby baroclinic radius (L_R). L_R characterizes regionally the size of long-lived eddies in the open ocean. The average value of L_R was calculated using the definition of Chelton et al. (1998) and the 7-year average (i.e., 2005 to 2012) of the World Ocean Database (Boyer et al., 2013). The resulting value is represented by the vertical dotted line in Figure 7. The shaded area represents L_R percentiles 10 and 90. This figure shows that TOEddies identifies structures whose size is comparable to L_R (around 60% of TOEddies radii are in the percentile range L_R 10 - 90), whereas this is not the case for META2017, for which less than 20% of radii are in this interval.

To ensure that the comparison of TOEddies and META2017 skill against LU16 loopers is as robust as possible in terms of measurement, TOEddies_rad statistics were used instead of TOEddies. Indeed, the TOEddies_rad and META2017 skills are obtained by considering equivalent eddy radii instead of eddy contours. Note here that the statistics for TOEddies and TOEddies_rad are very similar, only the skill decreases slightly. TOEddies_rad is 10% more efficient, and its error in eddy detection is 3 times lower than META2017 in terms of eddy collocation with LU16. The ability of TOEddies_rad and META2017 to encompass LU16 eddy centers as a function of eddy size is shown in Figure 8. The percentage of matches with LU16 increases while the percentage of matching errors decreases for both atlases as the size of the LU16 vortex increases. Both data sets are more effective at detecting small cyclones than small anticyclones, and large anticyclones than large cyclones.

It can be expected that there will be a minimum size of eddies detected on satellite altimetry maps. The ability of the two atlases, TOEddies and META2017, to match LU16 eddies as function of LU16 size is presented in Figure 8. It shows that for a 25-km radius (which represents the average radius of the LU16 loopers, Figure 5, and the average grid size of the altimetry maps) more than 65% of the eddies are identified by TOEddies

Table A2
Tracking Skill Statistics for Four Collocated Data Sets With LU16 Eddy Trajectories That Lasted at Least 1 Week

Data set	Limits	Trajectories tracked anti/cyclo (%)	% of trajectory network anti/cyclo (%)	Followed > 50% anti/cyclo (%)	Followed > 90% anti/cyclo (%)	Mean % time tracked anti/cyclo (%)	Trajectories errors anti/cyclo (%)
TOEAtlas	out	67/68	7/4	58/60	44/49	84/88	8/6
TOEAtlas	max	61/65	4/1	52/57	37/43	81/85	5/3
TOEAtlas_rad	max	58/63	6/4	49/54	34/40	81/84	4/5
META2017	max	48/58	3/7	35/41	26/27	73/70	9/8

Note. The percentage of trajectories tracked indicates the number of LU16 trajectories that are only associated with trajectories of the same polarity. The percentage of the trajectory network explains the percentage of trajectories poorly tracked in META2017 and properly tracked through the reconstruction of the first-order network in TOEddies. The columns > *50%* and > *90%* indicate the number of LU16 trajectories collocated with the eddies defined by the other atlases during, respectively, more than 50% and 90% of the life of LU16 eddies. The *mean tracking time* column gives the average percentage of collocation time between the LU16 loopers and the eddies of the other atlases expressed in terms of LU16 eddy life. The trajectory errors column indicates the number of trajectories associated, for at least 1 day, with an unmatched polarity eddy.

whereas they represent only 48% (52%) for the anticyclones (cyclones) in META2017. The 90% limit is reached for TOEddies for eddies with radii between 45 and 55 km, while it is 85–95 km (75–85 km) for anticyclones (cyclones) in META2017. In terms of detection errors (mismatching), they are less than 1% for anticyclones (cyclones) over 15 km (10 km) in the case of TOEddies, whereas for META2017, they become as small only for anticyclones (cyclones) larger than 30 km (70 km).

A3. Validation of Tracking Filtering

In this section, we examine the ability of the two atlases, TOEddies and META2017, to track eddies. This ability is measured by looking at the proportion of the eddy collocation of the two atlases with LU16 loopers that participate in a trajectory that lasts more than a week. The total number of LU16 trajectories used in the comparison is 431 for anticyclones and 414 for cyclones. The comparison is presented here for the three versions of our atlas where we vary either the type of contours defining the eddy area (the outer contour and the maximum velocity contour) or by applying the same method in the collocation with LU16 as used for META2017.

Eddy trajectory comparison statistics are presented in Table A2. Here skill is measured by the overall percentage of matching between the TOEddies or META2017 and LU16 trajectories. The percentage of trajectories tracked is computed as the percentage of LU16 eddy trajectories of each polarity associated, for at least 1 day, with TOEddies or META2017 eddy trajectories of the same polarity. The *trajectory network* column shows the percentage of LU16 trajectories erroneously matched by more than one eddy in META2017 or by a first-order network in TOEddies. The columns > *50%* and > *90%* indicate the number of LU16 trajectories collocated with the eddies defined by the other atlases during, respectively, more than 50% and 90% of lifetime of the LU16 eddies. The *mean tracking time* column gives the average percentage of collocation time between LU16 eddies and those of the other atlases, expressed in terms of LU16 lifetime. The error estimates correspond to the collocation of eddies of different polarities for at least 1 day.

The results show that the TOEddies skill improves when the outer eddy contour (R_{out}) instead of the maximum velocity contour (R_{Vmax}) is used to define the eddy perimeter. However, the associated mismatches are somewhat larger. Taking into account both definitions of eddy limits, between 60% and 70% of LU16 trajectories are tracked by TOEddies and between 50 and 60% of them are tracked for more than 50% of their lifetime. The reconstruction of a higher-order network is necessary for fewer than 10% of the trajectories successfully tracked. This could be a consequence of the LU16 filtering we performed before the validation processes. In fact, the merging and splitting of the eddies can cause sudden changes in the spin of the drifter and an increase in the radius of the LU16 loopers, a radius that can become greater than 300 km, the maximum limit we have set for them.

Using the radius for cross detection of structures gives results similar to those obtained using defined eddy perimeters. Table A2 shows that the greatest difference in skill is obtained for META2017. Indeed, META2017 identifies between 5% and 10% fewer trajectories than TOEddiesAtlas. Moreover, the percentages obtained for TOEddies indicate that trajectories that account for eddy merging and splitting are real and well reconstructed. On the other hand, the association of more than one META2017 trajectory with a LU16 trajectory

suggests that META2017 sometimes loses the true eddy track. This is clear when considering the collocation time with LU16 loopers. Indeed, while between 1/2 and 1/3 of the TOEddies network recovers almost all LU16 trajectories (i.e., > 90 %), this statistic is only 1/4 for META2017. Moreover, META2017 trajectories follow LU16 loopers 10% less than TOEddies. META2017 mismatch cases are also more numerous (by a factor of 2) than TOEddies cases.

Acknowledgments
The database produced for this paper and scripts to reproduce the main figures presented in the results are available at the following: https://vesg.ipsl.upmc.fr/thredds/catalog/IPSLFS/rlaxe/catalog.html?dataset=DatasetScanIPSLFS/rlaxe/Database_South_Atl.zip. The gridded altimeter products were produced by SSALTO/DUACS and distributed by the Copernicus Marine Environment Monitoring Service. The Mesoscale Eddy Trajectory Atlas products were produced by SSALTO/DUACS and distributed by AVISO+ (http://www.aviso.altimetry.fr/) with support from CNES, in collaboration with Oregon State University with support from NASA. The Looper trajectory segments in Global Drifter Program data are available at http://www.aoml.noaa.gov/phod/loopers/. The development of this work was made possible through the scientific visits of A. C., C. P., and R. L. at IMARPE (Peru). R. L. had financial support from the Agence Nationale de la Recherche via the international mobility LabexMer, grant ANR-10-LABX-19-01 for this visit. This work was supported by the European Union's Horizon 2020 research and innovation program under grant agreement 633211 (AtlantOS), a CNES-TOSCA research grant for S. S. and R. L. and the 11-ANR-56-004 grant for S. S. and B. B. by the CNRS and INSU for B. B.; IRD for A. C.; and ANR DynEd Atlas for A. C., C. P., and A. S. We also acknowledge the mesoscale calculation server CICLAD (http://ciclad-web.ipsl.jussieu.fr) dedicated to Institut Pierre Simon Laplace modeling effort for technical and computational support. The authors thank the three anonymous reviewers for their constructive suggestions and relevant questions that improved the quality of the manuscript.

References

Arhan, M., Mercier, H., & Lutjeharms, J. R. E. (1999). The disparate evolution of three Agulhas rings in the South Atlantic Ocean. *Journal of Geophysical Research*, *104*(C9), 20,987–21,005. https://doi.org/10.1029/1998JC900047

Arhan, M., Speich, S., Messager, C., Dencausse, G., Fine, R., & Boye, M. (2011). Anticyclonic and cyclonic eddies of subtropical origin in the subantarctic zone south of Africa. *Journal of Geophysical Research (1978–2012)*, *116*, C11004. https://doi.org/2011JC007140

Ashkezari, M. D., Hill, C. N., Follett, C. N., Forget, G., & Follows, M. J. (2016). Oceanic eddy detection and lifetime forecast using machine learning methods. *Geophysical Research Letters*, *43*, 12,234–12,241. https://doi.org/10.1002/2016GL071269

Baker-Yeboah, S., Byrne, D. A., & Watts, D. R. (2010). Observations of mesoscale eddies in the South Atlantic Cape Basin: Baroclinic and deep barotropic eddy variability. *Journal of Geophysical Research*, *115*, C12069. https://doi.org/10.1029/2010JC006236

Ballegooyen, R. C., Gründlingh, M. L., & Lutjeharms, J. R. (1994). Eddy fluxes of heat and salt from the southwest Indian Ocean into the southeast Atlantic Ocean: A case study. *Journal of Geophysical Research*, *99*(C7), 14,053–14,070.

Beal, L. M., & Elipot, S. (2016). Broadening not strengthening of the Agulhas Current since the early 1990s. *Nature*, *540*(7634), 570–573.

Beal, L. M., Ruijter, W. P. M. D., Biastoch, A., Zahn, R., Cronin, M., Hermes, J., et al. (2011). On the role of the Agulhas system in ocean circulation and climate. *Nature*, *472*(7344), 429–436. https://doi.org/10.1038/nature09983 authors No 5 to 19 are members of the Working Group.

Biastoch, A., & Böning, C. W. (2013). Anthropogenic impact on Agulhas leakage. *Geophysical Research Letters*, *40*, 1138–1143. https://doi.org/10.1002/grl.50243

Biastoch, A., Böning, C. W., & Lutjeharms, J. R. E. (2008). Agulhas leakage dynamics affects decadal variability in Atlantic overturning circulation. *Nature*, *456*, 489–492. https://doi.org/doi:10.1038/nature07426

Biastoch, A., Lutjeharms, J. R. E., Böning, C. W., & Scheinert, M. (2008). Mesoscale perturbations control inter-ocean exchange south of Africa. *Geophysical Research Letters*, *35*, l20602. https://doi.org/10.1029/2008GL035132

Boebel, O., Lutjeharms, J., Schmid, C., Zenk, W., Rossby, T., & Barron, C. (2003). The Cape Cauldron: A regime of turbulent inter-ocean exchange. *Deep Sea Research Part II: Topical Studies in Oceanography*, *50*(1), 57–86.

Boebel, O., Rossby, T., Lutjeharms, J., Zenk, W., & Barron, C. (2003). Path and variability of the Agulhas Return Current. *Deep Sea Research Part II: Topical Studies in Oceanography*, *50*(1), 35–56.

Boyer, T. P., Antonov, J. I., Baranova, O. K., Coleman, C., Garcia, H. E., Grodsky, A., et al. (2013). World ocean database.

Byrne, D. A., Gordon, A. L., & Haxby, W. F. (1995). Agulhas eddies: A synoptic view using Geosat ERM data. *Journal of Physical Oceanography*, *25*(5), 902–917. https://doi.org/10.1175/1520-0485(1995)025<0902:AEASVU>2.0.CO;2

Capet, A., Mason, E., Rossi, V., Troupin, C., Faugère, Y., Pujol, I., & Pascual, A. (2014). Implications of refined altimetry on estimates of mesoscale activity and eddy-driven offshore transport in the Eastern Boundary Upwelling Systems. *Geophysical Research Letters*, *41*, 7602–7610. https://doi.org/10.1002/2014GL061770

Carton, X. (2001). Hydrodynamical Modeling of Oceanic Vortices. *Surveys in Geophysics*, *22*(3), 179–263. https://doi.org/10.1023/A:1013779219578

Casanova-Masjoan, M., Pelegrí, J., Sangrà, P., Martínez, A., Grisolía-Santos, D., Pérez-Hernández, M. D., & Hernández-Guerra, A. (2017). Characteristics and evolution of an Agulhas ring. *Journal of Geophysical Research: Oceans*, *122*, 7049–7065. https://doi.org/10.1002/2017JC012969

Chaigneau, A., Eldin, G., & Dewitte, B. (2009). Eddy activity in the four major upwelling systems from satellite altimetry (1992–2007). *Progress in Oceanography*, *83*(1), 117–123.

Chaigneau, A., Gizolme, A., & Grados, C. (2008). Mesoscale eddies off Peru in altimeter records: Identification algorithms and eddy spatio-temporal patterns. *Progress in Oceanography*, *79*(2), 106–119.

Chaigneau, A., Marie, L. T., Gérard, E., Carmen, G., & Oscar, P. (2011). Vertical structure of mesoscale eddies in the eastern South Pacific Ocean: A composite analysis from altimetry and Argo profiling floats. *Journal of Geophysical Research*, *116*, C11025. https://doi.org/10.1029/2011JC007134

Chaigneau, A., & Pizarro, O. (2005). Eddy characteristics in the eastern South Pacific. *Journal of Geophysical Research*, *110*, C06005. https://doi.org/10.1029/2004JC002815

Chelton, D. B., deSzoeke, R. A., Schlax, M. G., El Naggar, K., & Siwertz, N. (1998). Geographical Variability of the First Baroclinic Rossby Radius of Deformation. *Journal of Physical Oceanography*, *28*(3), 433–460. https://doi.org/10.1175/1520-0485(1998)028<0433:GVOTFB>2.0.CO;2

Chelton, D. B., Schlax, M. G., & Samelson, R. M. (2011). Global observations of nonlinear mesoscale eddies. *Progress in Oceanography*, *91*(2), 167–216. https://doi.org/10.1016/j.pocean.2011.01.002

Chelton, D. B., Schlax, M. G., Samelson, R. M., & de Szoeke, R. A. (2007). Global observations of large oceanic eddies. *Geophysical Research Letters*, *34*, L15606. https://doi.org/10.1029/2007GL030812

Cipollone, A., Masina, S., Storto, A., & Iovino, D. (2017). Benchmarking the mesoscale variability in global ocean eddy-permitting numerical systems. *Ocean Dynamics*, *67*(10), 1313–1333.

Cresswell, G. R. (1982). The coalescence of two East Australian Current warm-core eddies. *Science*, *215*(4529), 161–164.

Cushman-Roisin, B., Tang, B., & Chassignet, E. P. (1990). Westward motion of mesoscale eddies. *Journal of Physical Oceanography*, *20*(5), 758–768.

Dencausse, G., Arhan, M., & Speich, S. (2010a). Routes of Agulhas rings in the southeastern Cape Basin. *Deep Sea Research Part I: Oceanographic Research Papers*, *57*(11), 1406–1421.

Dencausse, G., Arhan, M., & Speich, S. (2010b). Spatio-temporal characteristics of the Agulhas Current Retroflection. *Deep Sea Research Part I: Oceanographic Research Papers*, *57*(11), 1392–1405.

Doglioli, A. M., Blanke, B., Speich, S., & Lapeyre, G. (2007). Tracking coherent structures in a regional ocean model with wavelet analysis: Application to Cape Basin eddies. *Journal of Geophysical Research*, *112*, C05043. https://doi.org/10.1029/2006JC003952

Donohue, K. A., Firing, E., & Beal, L. (2000). Comparison of three velocity sections of the Agulhas current and Agulhas undercurrent. *Journal of Geophysical Research*, *105*(C12), 28,585–28,593. https://doi.org/10.1029/1999JC000201

Drijfhout, S. S. (2003). Why anticyclones can split. *Journal of Physical Oceanography*, *33*(8), 1579–1591.
Duacs/AVISO+ (2014). A new version of SSALTO/Duacs products available in April 2014. Version 1.1, CNES. [Available at http://www.aviso.altimetry.fr/fileadmin/documents/data/duacs/Duacs2014.pdf.].
Duacs/AVISO+ (2015). SSALTO/DUACS user handbook:(M) SLA and (M) ADT near-real time and delayed time products. *CLS-DOS-NT-06-034*, *6*, 74.
Duacs/AVISO+ (2017). Mesoscale eddy trajectory Atlas product handbook. SALP-MU-P-EA-23126-CLS.
Duncombe Rae, C. M. (1991). Agulhas retroflection rings in the South Atlantic Ocean: An overview. *South African Journal of Marine Science*, *11*(1), 327–344. https://doi.org/10.2989/025776191784287574
Edelsbrunner, H., & Harer, J. (2010). *Computational topology: An introduction*. USA: American Mathematical Soc.
Edelsbrunner, H., Letscher, D., & Zomorodian, A. (2002). Topological persistence and simplification. *Discrete and Computational Geometry*, *28*, 511–533.
Elipot, S., & Beal, L. M. (2015). Characteristics, energetics, and origins of Agulhas Current meanders and their limited influence on ring shedding. *Journal of Physical Oceanography*, *45*(9), 2294–2314. https://doi.org/10.1175/JPO-D-14-0254.1
Faghmous, J. H., Frenger, I., Yao, Y., Warmka, R., Lindell, A., & Kumar, V. (2015). A daily global mesoscale ocean eddy dataset from satellite altimetry. *Scientific Data*, *2*, 150,028. https://doi.org/10.1038/sdata.2015.28
Frenger, I., Münnich, M., Gruber, N., & Knutti, R. (2015). Southern ocean eddy phenomenology. *Journal of Geophysical Research: Oceans*, *120*, 7413–7449. https://doi.org/10.1002/2015JC011047
Garzoli, S. L., Richardson, P. L., Duncombe Rae, C. M., Fratantoni, D. M., Goñi, G. J., & Roubicek, A. J. (1999). Three Agulhas rings observed during the Benguela current experiment. *Journal of Geophysical Research*, *104*(C9), 20,971–20,985. https://doi.org/10.1029/1999JC900060
Goni, G., Garzoli, S., Roubicek, A., Olson, D., & Brown, O. (1997). Agulhas ring dynamics from TOPEX/POSEIDON satellite altimeter data. *Journal of Marine Research*, *55*, 861–883. https://doi.org/10.1357/0022240973224175
Gordon, A. L. (1985). Indian-Atlantic transfer of thermocline water at the Agulhas retroflection. *Science*, *227*, 1030–1034.
Gordon, A. L., & Haxby, W. F. (1990). Agulhas eddies invade the South Atlantic: Evidence from Geosat altimeter and shipboard conductivity-temperature-depth survey. *Journal of Geophysical Research*, *95*(C3), 3117–3125.
Gordon, A. L., Weiss, R., Smethie, W., & Warner, M. (1992). Thermocline and intermediate water communication between the South Atlantic and Indian Oceans. *Journal of Geophysical Research*, *97*, 7223–7240.
Griffa, A., Lumpkin, R., & Veneziani, M. (2008). Cyclonic and anticyclonic motion in the upper ocean. *Geophysical Research Letters*, *35*, l01608. https://doi.org/10.1029/2007GL032100
Guerra, L. A. A., Paiva, A. M., & Chassignet, E. P. (2018). On the translation of Agulhas rings to the western South Atlantic Ocean. *Deep Sea Research Part I: Oceanographic Research Papers*, *139*, 104–113.
Haller, G., & Beron-Vera, F. J. (2013). Coherent Lagrangian vortices: The black holes of turbulence. *Journal of Fluid Mechanics*, *731*.
Halo, I., Backeberg, B., Penven, P., Ansorge, I., Reason, C., & Ullgren, J. (2014). Eddy properties in the Mozambique Channel: A comparison between observations and two numerical ocean circulation models. *Deep Sea Research Part II: Topical Studies in Oceanography*, *100*, 38–53.
Herbette, S., Morel, Y., & Arhan, M. (2004). Subduction of a surface vortex under an outcropping front. *Journal of Physical Oceanography*, *34*(7), 1610–1627.
Hernandez, F., Le Traon, P.-Y., & Morrow, R. (1995). Mapping mesoscale variability of the Azores Current using TOPEX/POSEIDON and ERS 1 altimetry, together with hydrographic and Lagrangian measurements. *Journal of Geophysical Research*, *100*(C12), 24,995–25,006. https://doi.org/10.1029/95JC02333
Ioannou, A., Stegner, A., Le Vu, B., Taupier-Letage, I., & Speich, S. (2017). Dynamical evolution of intense Ierapetra eddies on a 22 year long period. *Journal of Geophysical Research: Oceans*, *122*, 9276–9298. https://doi.org/10.1002/2017JC013158
Isern-Fontanet, J., García-Ladona, E., & Font, J. (2006). Vortices of the mediterranean sea: An altimetric perspective. *Journal of Physical Oceanography*, *36*(1), 87–103.
Isoda, Y. (1994). Warm eddy movements in the eastern Japan Sea. *Journal of Oceanography*, *50*(1), 1–15.
Le Vu, B., Stegner, A., & Arsouze, T. (2018). Angular Momentum Eddy Detection and tracking Algorithm (AMEDA) and its application to coastal eddy formation. *Journal of Atmospheric and Oceanic Technology*, *35*(4), 739–762.
Lehahn, Y., d'Ovidio, F., Lévy, M., Amitai, Y., & Heifetz, E. (2011). Long range transport of a quasi isolated chlorophyll patch by an Agulhas ring. *Geophysical Research Letters*, *38*, L16610. https://doi.org/10.1029/2011GL048588
Lumpkin, R. (2016). Global characteristics of coherent vortices from surface drifter trajectories. *Journal of Geophysical Research: Oceans*, *121*, 1306–1321. https://doi.org/10.1002/2015JC011435
Lumpkin, R., & Pazos, M. (2007). Measuring surface currents with Surface Velocity Program drifters: The instrument, its data, and some recent results. *Lagrangian analysis and prediction of coastal and ocean dynamics* (pp. 39–67).
Lutjeharms, J. R. E. (2006). *The Agulhas Current* (342 pp.). Berlin: Springer-Verlag.
Lutjeharms, J. R. E., & Ballegooyen, R. C. V. (1988). The retroflection of the Agulhas Current. *Journal of Physical Oceanography*, *18*(11), 1570–1583.
Lutjeharms, J., & Gordon, A. (1987). Shedding of an Agulhas ring observed at sea. *Nature*, *325*(6100), 138–140.
Mason, E., Pascual, A., & McWilliams, J. C. (2014). A new sea surface height–based code for oceanic Mesoscale Eddy tracking. *Journal of Atmospheric and Oceanic Technology*, *31*(5), 1181–1188. https:/doi.org/10.1175/JTECH-D-14-00019.1
Matsuoka, D., Araki, F., Inoue, Y., & Sasaki, H. (2016). A new approach to ocean Eddy detection, tracking, and event visualization–application to the Northwest Pacific Ocean. *Procedia Computer Science*, *80*, 1601–1611.
McDonagh, E. L., Heywood, K. J., & Meredith, M. P. (1999). On the structure, paths, and fluxes associated with Agulhas rings. *Journal of Geophysical Research*, *104*(C9), 21,007–21,020.
McWilliams, J. C. (1985). Submesoscale, coherent vortices in the ocean. *Reviews of Geophysics*, *23*(2), 165–182.
Melander, M., Zabusky, N., & McWilliams, J. (1988). Symmetric vortex merger in two dimensions: Causes and conditions. *Journal of Fluid Mechanics*, *195*, 303–340.
Mkhinini, N., Coimbra, A. L. S., Stegner, A., Arsouze, T., Taupier-Letage, I., & Béranger, K. (2014). Long-lived mesoscale eddies in the eastern Mediterranean Sea: Analysis of 20 years of AVISO geostrophic velocities. *Journal of Geophysical Research: Oceans*, *119*, 8603–8626. https:/doi.org/10.1002/2014JC010176
Nencioli, F., Dong, C., Dickey, T., Washburn, L., & McWilliams, J. C. (2010). A vector geometry–based Eddy detection algorithm and its application to a high-resolution numerical model product and high-frequency radar surface velocities in the Southern California Bight. *Journal of Atmospheric and Oceanic Technology*, *27*(3), 564–579. https:/doi.org/10.1175/2009JTECHO725.1

Okubo, A. (1970). Horizontal dispersion of floatable particles in the vicinity of velocity singularities such as convergences, *Deep sea research and oceanographic abstracts* (vol. 17, pp. 445–454), Netherlands: Elsevier.
Olson, D. B., & Evans, R. H. (1986). Rings of the Agulhas current. *Deep Sea Research Part A. Oceanographic Research Papers*, *33*(1), 27–42.
Paul, M., van de Flierdt, T., Rehkämper, M., Khondoker, R., Weiss, D., Lohan, M. C., & Homoky, W. B. (2015). Tracing the Agulhas leakage with lead isotopes. *Geophysical Research Letters*, *42*, 8515–8521. https://doi.org/10.1002/2015GL065625
Pegliasco, C., Chaigneau, A., & Morrow, R. (2015). Main eddy vertical structures observed in the four major Eastern boundary upwelling systems. *Journal of Geophysical Research: Oceans*, *120*, 6008–6033. https://doi.org/10.1002/2015jc010950
Penven, P., Echevin, V., Pasapera, J., Colas, F., & Tam, J. (2005). Average circulation, seasonal cycle, and mesoscale dynamics of the Peru current system: A modeling approach. *Journal of Geophysical Research*, *110*, C10021. https://doi.org/10.1029/2005JC002945
Penven, P., Lutjeharms, J. R. E., & Florenchie, P. (2006). Madagascar: A pacemaker for the Agulhas current system? *Geophysical Research Letters*, *33*, L17609. https://doi.org/10.1029/2006GL026854
Pujol, M.-I., Faugère, Y., Taburet, G., Dupuy, S., Pelloquin, C., Ablain, M., & Picot, N. (2016). DUACS DT2014: The new multi-mission altimeter data set reprocessed over 20 years. *Ocean Science*, *12*(5), 1067–1090.
Qiu-Yang, L., Sun, L., & Sheng-Fu, L. (2016). Gem: A dynamic tracking model for mesoscale eddies in the ocean. *Ocean Science*, *12*(6), 1249.
Rhines, P. B. (1975). Waves and turbulence on a beta-plane. *Journal of Fluid Mechanics*, *69*(3), 417–443.
Rio, M., Guinehut, S., & Larnicol, G. (2011). New CNES-CLS09 global mean dynamic topography computed from the combination of GRACE data, altimetry, and in situ measurements. *Journal of Geophysical Research*, *116*, C07018. https://doi.org/10.1029/2010JC006505
Rio, M.-H., Mulet, S., & Picot, N. (2014). Beyond GOCE for the ocean circulation estimate: Synergetic use of altimetry, gravimetry, and in situ data provides new insight into geostrophic and Ekman currents. *Geophysical Research Letters*, *41*, 8918–8925. https://doi.org/10.1002/2014GL061773
Rouault, M., Penven, P., & Pohl, B. (2009). Warming in the Agulhas current system since the 1980's. *Geophysical Research Letters*, *36*, L12602. https://doi.org/10.1029/2009GL037987
Rühs, S., Durgadoo, J. V., Behrens, E., & Biastoch, A. (2013). Advective timescales and pathways of Agulhas leakage. *Geophysical Research Letters*, *40*, 3997–4000. https://doi.org/10.1002/grl.50782
Ruijter, W. D., Biastoch, A., Drijfhout, S., Lutjeharms, J., Matano, R., Pichevin, T., et al. (1999). IndianâĂŘAtlantic interocean exchange: Dynamics, estimation and impact. *Journal of Geophysical Research (1978–2012)*, *104*(C9), 20,885–20,910.
Sangrà, P., Pelegrí, J. L., Hernández-Guerra, A., Arregui, I., Martín, J. M., Marrero-Díaz, A., et al. (2005). Life history of an anticyclonic eddy. *Journal of Geophysical Research*, *C03021*. https://doi.org/10.1029/2004JC002526
Schlax, M. G., & Chelton, D. B. (2016). The "growing method" of eddy identification and tracking in two and three dimensions.
Schouten, M. W., de Ruijter, W. P. M., & van Leeuwen, P. J. (2002). Upstream control of Agulhas Ring shedding. *Journal of Geophysical Research*, *107*, 23–1–23–11. https://doi.org/10.1029/2001JC000804
Schouten, M. W., de Ruijter, W. P. M., van Leeuwen, P. J., & Lutjeharms, J. R. E. (2000). Translation, decay and splitting of Agulhas rings in the southeastern Atlantic Ocean. *Journal of Geophysical Research*, *105*, 21,913–21,925. https://doi.org/10.1029/1999JC000046
Schultz Tokos, K. L., Hinrichsen, H.-H., & Zenk, W. (1994). Merging and migration of two meddies. *Journal of Physical Oceanography*, *24*(10), 2129–2141.
Simmons, H. L., & Nof, D. (2000). Islands as eddy splitters. *Journal of Marine Research*, *58*(6), 919–956.
Smith, W., & Sandwell, D. (1997). Global sea floor topography from satellite altimetry and ship depth soundings. *Science*, *277*(5334), 1956–1962.
Souza, J. M. A. C., de Boyer Montégut, C., Cabanes, C., & Klein, P. (2011). Estimation of the Agulhas ring impacts on meridional heat fluxes and transport using ARGO floats and satellite data. *Geophysical Research Letters*, *28*, L21602. https://doi.org/10.1029/2011GL049359
Souza, J. M. A. C. D., De Boyer Montegut, C., & Le Traon, P.-Y. (2011). Comparison between three implementations of automatic identification algorithms for the quantification and characterization of mesoscale eddies in the south atlantic ocean. *Ocean Science*, *7*(3), 317–334.
Stammer, D. (1997). Global characteristics of ocean variability estimated from regional TOPEX/POSEIDON altimeter measurements. *Journal of Physical Oceanography*, *27*(8), 1743–1769.
Tierny, J., Favelier, G., Levine, J. A., Gueunet, C., & Michaux, M. (2018). The topology toolkit. *IEEE Transactions on Visualization and Computer Graphics*, *24*(1), 832–842.
van Sebille, E., Beal, L. M., & Johns, W. E. (2011). Advective time scales of Agulhas leakage to the North Atlantic in surface drifter observations and the 3D OFES model. *Journal of Physical Oceanography*, *41*(5), 1026–1034.
van Sebille, E., & van Leeuwen, P. J. (2007). Fast northward energy transfer in the Atlantic due to Agulhas rings. *Journal of Physical Oceanography*, *37*(9), 2305–2315.
van Sebille, E., Van Leeuwen, P. J., Biastoch, A., & de Ruijter, W. P. (2010). On the fast decay of Agulhas rings. *Journal of Geophysical Research*, *115*, C03010. https://doi.org/10.1029/2009JC005585
Veneziani, M., Griffa, A., Reynolds, A. M., & Mariano, A. J. (2004). Oceanic turbulence and stochastic models from subsurface lagrangian data for the Northwest Atlantic Ocean. *Journal of Physical Oceanography*, *34*, 1884–1906. https://doi.org/10.1175/1520-0485(2004)034<1884:OTASMF>2.0.CO;2
Villar, E., Farrant, G. K., Follows, M., Garczarek, L., Speich, S., Audic, S., et al. (2015). Environmental characteristics of Agulhas rings affect interocean plankton transport. *Science*, *348*(6237), 1261,447.
Wang, Y., Beron-Vera, F., & Olascoaga, M. (2016). The life cycle of a coherent lagrangian Agulhas ring. *Journal of Geophysical Research: Oceans*, *121*, 3944–3954. https://doi.org/10.1002/2015JC011620
Wang, Y., Olascoaga, M., & Beron-Vera, F. (2015). Coherent water transport across the South Atlantic. *Geophysical Research Letters*, *42*, 4072–4079.
Weijer, W., De Ruijter, W. P., & Dijkstra, H. A. (2001). Stability of the Atlantic overturning circulation: Competition between Bering Strait freshwater flux and Agulhas heat and salt sources. *Journal of Physical Oceanography*, *31*(8), 2385–2402.
Weijer, W., de Ruijter, W. P., Dijkstra, H. A., & Van Leeuwen, P. J. (1999). Impact of interbasin exchange on the Atlantic overturning circulation. *Journal of Physical Oceanography*, *29*(9), 2266–2284.
Weijer, W., De Ruijter, W. P., Sterl, A., & Drijfhout, S. S. (2002). Response of the Atlantic overturning circulation to South Atlantic sources of buoyancy. *Global and Planetary Change*, *34*(3), 293–311.
Weiss, J. (1991). The dynamics of enstrophy transfer in two-dimensional hydrodynamics. *Physica D: Nonlinear Phenomena*, *48*(2-3), 273–294.
Williams, S., Petersen, M., Bremer, P.-T., Hecht, M., Pascucci, V., Ahrens, J., et al. (2011). Adaptive extraction and quantification of geophysical vortices. *IEEE Transactions on Visualization and Computer Graphics*, *17*(12), 2088–2095.
Wunsch, C. (1999). Where do ocean eddy heat fluxes matter? *Journal of Geophysical Research*, *104*(C6), 13,235–13,249.
Yi, J., Du, Y., He, Z., & Zhou, C. (2014). Enhancing the accuracy of automatic eddy detection and the capability of recognizing the multi-core structures from maps of sea level anomaly. *Ocean Science*, *10*(1), 39.
Zheng, S., Du, Y., Li, J., & Cheng, X. (2015). Eddy characteristics in the South Indian Ocean as inferred from surface drifters. *Ocean Science*, *11*(3), 361–371. https://doi.org/10.5194/os-11-361-2015